From Department of Molecular Medicine and Surgery
Karolinska Institutet, Stockholm, Sweden

Preoperative localisation of parathyroid adenoma in primary hyperparathyroidism using ^{99m}Tc-sestamibi SPECT/CT: an evolving scanning protocol

Patricia Sandqvist

Stockholm 2022

Published by Karolinska Institutet.
Printed by Universitetsservice US-AB, 2022

ISBN 978-91-8016-519-8
Cover illustration: Above, arteriogram (invasive method) performed in 1954 by Sven Ivar Seldinger with indirect signs of a parathyroid adenoma (deflecting vessels). This image was originally published in Acta Radiologica (1). Below, ^{99m}Tc-sestamibi SPECT/CT with contrast-enhanced CT in arterial phase (non-invasive method) performed at our department, illustrating the corresponding arteries but with direct visualisation of a contrast-enhancing and ^{99m}Tc-sestamibi accumulating parathyroid adenoma.

Preoperative localisation of parathyroid adenoma in primary hyperparathyroidism using ^{99m}Tc-sestamibi SPECT/CT: an evolving scanning protocol

Akademisk avhandling

som för avläggande av medicine doktorsexamen vid Karolinska Institutet offentligen försvaras i Skandiasalen, QA31, plan 01, Karolinska vägen 37A,"Gamla" Astrid Lindgrens barnsjukhus, Solna
Fredagen den 29 april 2022, kl. 09.00

av

Patricia Sandqvist

Principal Supervisor:
Associate Professor Alejandro Sanchez-Crespo
Karolinska Institutet
Department of Oncology and Pathology

Co-supervisor(s):
Professor Anders Sundin
Uppsala University
Department of Surgical Science, Radiology

Associate Professor Inga-Lena Nilsson
Karolinska Institutet
Department of Molecular Medicine and Surgery

Ph.D. Per Grybäck
Karolinska Institutet
Department of Molecular Medicine and Surgery

Opponent:
Professor Håkan Geijer
Örebro University
Department of Medical Sciences

Examination Board:
Professor Katrine Riklund
Umeå University
Department of Radiation Sciences

Associate Professor Ivan Shabo
Karolinska Institutet
Department of Molecular Medicine and Surgery

Professor Peter Bernhardt
Göteborg University
Department of Radiation Physics

To my father professor Stig A. Larsson who was a pioneer in the development of SPECT-detectors in the late 1970s. You taught me so much about everything from salmon fishing to electronics.

To my mother Anita Vestberg Olofsson for always believing in me and for all the comfort during gloomy times.

To my beloved wife Camilla Sandqvist for all your patience, support and all the joyous breaks during this arduous process.

POPULAR SCIENCE SUMMARY OF THE THESIS

The calcium ion has several important functions in the human body. In addition to its crucial contribution to the strength of bone structures, it is also involved in many physiological processes like regulating the muscle tension, nerve signalling and many other internal messenger systems of the cells. The concentration of calcium ions is monitored and regulated within narrow limits for these systems to work. The parathyroid glands, usually four, play an important role in that regulation by means of the parathyroid hormone (PTH). PTH acts on its target organs, the bones and kidneys, and indirectly by activation of vitamin D, to elevate the calcium concentration in the blood. When cells of the parathyroid glands, through sensors on their surface, find the calcium level low, PTH is synthesised and secreted by these cells.

In primary hyperparathyroidism (pHPT) one or several of the parathyroid glands starts to release excessive amounts of PTH relative to the calcium concentration, resulting in too high calcium levels. In most cases (85-90%), this is caused by a benign tumour, an adenoma, sometimes by multiple adenomas and rarely (<1%) by parathyroid cancer. Continuous excessive PTH excretion may cause osteoporosis with skeletal pain and fractures. The high circulating concentration of calcium ions in blood can cause renal insufficiency, sometimes as a result of kidney stone disease. Symptoms such as muscle weakness and general fatigue are common. Cognitive impairment and depression occur, and comorbidities are overrepresented, such as irreversible hypertension and cardiovascular disease.

Primary hyperparathyroidism is the third most common endocrine disease following diabetes and thyroid diseases. The diagnosis is obtained by biochemical analysis and is often detected by chance on blood sampling performed for other reasons than pHPT. The only definite cure is surgical removal of all hyperfunctioning parathyroid glands but leaving enough normal parathyroid tissue in place to avoid hypoparathyroidism. According to the report of 2020 from the Scandinavian Quality Register for Thyroid, Parathyroid and Adrenal surgery (SQRTPA) approximately 900 patients undergo parathyroid surgery in Sweden annually, which has been fairly constant over the past decade. Primary hyperparathyroidism is more common in women (75% of the patients) and in elderly, with a mean age at surgery of 62 years.

Due to the complicated embryological development of the parathyroid glands, their number and location may vary. The size of a pathologic parathyroid is usually less than one cm. A prerequisite in order to simplify and minimise the surgical procedure, reduce the time in the operating room and the risk of complications, is therefore accurate preoperative localisation of the enlarged gland (or glands). There are currently several imaging methods used for this purpose, ultrasonography and ^{99m}Tc-sestamibi SPECT/CT, performed in the nuclear medicine department. ^{99m}Tc, meta-stable Technetium-99, is a gamma emitting isotope used to label sestamibi, a lipophilic positively charged compound that accumulates in hyperfunctioning parathyroid glands, but also in some other tissues. SPECT (Single Photon Emission Computed Tomography) utilises a gamma radiation detector that is rotated around the patient

and the acquired data are reconstructed in transversal low-resolution images of the regional radioactivity distribution in the tissues. In the computed tomography (CT) scanner an X-ray tube is rotated around the patient producing high-resolution anatomical transversal images of the X-ray attenuation in the tissues. For contrast enhancement an iodine-based contrast agent is administered intravenously to increase the attenuation differences in the tissues. Contrast agents accumulate largely depending on the degree of tissue perfusion (vascular richness) and thus, increase the image contrast between tissues with high perfusion (e.g., parathyroid glands) compared to those with low perfusion.

In this thesis, we have analysed the performance of various ^{99m}Tc-sestamibi SPECT/CT components including: ^{99m}Tc-sestamibi SPECT, CT with and without contrast enhancement and different contrast enhancement phases acquired at different time-points after administration of the contrast agent. The aim of this thesis was to develop an optimised clinical ^{99m}Tc-sestamibi SPECT/CT examination protocol for preoperative localisation of hyperactive / enlarged parathyroid glands and assess its performance in comparison with other existing protocols and imaging modalities.

POPULÄRVETENSKAPLIG SAMMANFATTNING AV AVHANDLINGEN

Kalcium har flera viktiga funktioner i människokroppen. Förutom dess avgörande bidrag till styrkan hos benstrukturer, är det också involverat i många fysiologiska processer som att reglera muskelspänning, nervsignalering och många andra interna budbärarsystem i cellerna. Koncentrationen av kalciumjoner övervakas och regleras inom snäva gränser för att dessa system ska fungera. Bisköldkörtlarna (oftast fyra till antalet) spelar en viktig roll i denna reglering genom bisköldkörtelhormonet (PTH). PTH verkar på sina målorgan skelett och njurar och indirekt via aktivering av D-vitamin, för att höja kalciumkoncentrationen. Om celler i bisköldkörtlarna genom sensorer på ytan finner att kalciumnivån är låg, tillverkar och frigör de PTH för att höja den.

Vid primär hyperparatyreoidism (pHPT) börjar en eller flera bisköldkörtlar att släppa ut för stora mängder PTH, relativt kalciumkoncentrationen framkallande en alltför hög kalciumnivå. I de flesta fall (85-90%) orsakas detta av en godartad tumör, i vissa fall av flerkörtelsjukdom och sällan (<1%) av bisköldkörtelcancer. Förhöjt PTH kan orsaka benskörhet med skelettsmärta och frakturer, njursvikt och njursten. Symptom som muskelsvaghet och allmän trötthet är vanliga. Kognitiv försämring och depression förekommer liksom samsjuklighet som kroniskt förhöjt blodtryck och hjärt-kärlsjukdom.

Primär hyperparatyreoidism är den tredje vanligaste endokrina (hormonella) sjukdomen efter diabetes och sköldkörtelsjukdomar. Diagnosen erhålls genom biokemisk analys och upptäcks ofta av en slump vid blodprov som tas av andra skäl än pHPT. Det enda säkra botemedlet som är känt idag är att kirurgiskt avlägsna alla bisköldkörtlar med hormonell överproduktion och lämna kvar tillräckligt med normal bisköldkörtelvävnad för att undvika underfunktion (hypoparatyreoidism). Enligt en rapport utkommen 2020 från skandinaviska kvalitetsregistret över thyroidea-, parathyreoidea- och binjurekirurgi (SQRTPA), har ett relativt konstant antal om cirka 900 patienter årligen i Sverige genomgått kirurgi för pHPT under det senaste decenniet. Sjukdomen är vanligare bland kvinnor (75% av patienterna) och bland äldre, med en medelålder vid kirurgi på ca 62 år.

På grund av den komplicerade embryologiska utvecklingen av bisköldkörtlarna kan deras antal och lokalisation variera. De sjuka bisköldkörtlarna är ofta mindre än en cm i storlek. En förutsättning för att förenkla och minimera det kirurgiska ingreppet, minska operationstiden och risken för komplikationer är därför noggrann preoperativ lokalisering av den förstorade körteln (eller körtlarna). Det finns idag flera avbildningsmetoder som används för detta ändamål, ultraljud (vanligen utförd av kirurg) och ^{99m}Tc-sestamibi SPECT/CT utförd på nuklearmedicinska avdelningen. ^{99m}Tc, metastabil teknetium-99, är en gamma-emitterande isotop som används för att märka sestamibi, en lipofil positivt laddad förening som ackumuleras i överproducerande bisköldkörtlar, men även i vissa andra vävnader.

SPECT (Single Photon Emission Computed Tomography) är en avbildningsmetod där en gammastrålningsdetektor roterar kring en patient och producerar funktionella lågupplösta

tvärsnittsbilder av den regionala fördelningen av radioaktiviteten. CT (Computed Tomography) också kallad skiktröntgen är en röntgenmetod som producerar högupplösta anatomiska tvärsnittsbilder. CT kan kontrastförstärkas genom intravenös injektion av jodkontrastmedel som bromsar röntgenstrålningen. Kontrastmedel ackumuleras till stor del beroende på graden av vävnadens genomblödning (kärlrikedom) och ökar därmed den bildmässiga kontrasten mellan olika vävnader med hög genomblödning (t.ex. bisköldkörtlar) jämfört med andra med låg genomblödning.

I denna avhandling har vi analyserat prestandan hos de olika ^{99m}Tc-sestamibi SPECT/CT-komponenterna inkluderande: ^{99m}Tc-sestamibi SPECT, CT utan och med kontrastförstärkning samt i olika kontrastförstärkningsfaser d.v.s. att CT utförs vid olika tidpunkter efter kontrastmedelsinjektionen.

Syftet har varit att utveckla ett optimerat kliniskt ^{99m}Tc-sestamibi SPECT/CT-undersökningsprotokoll för lokalisering av hormonöverproducerande bisköldkörtlar och att utvärdera dess avbildningsprestanda i jämförelse med andra befintliga undersökningsprotokoll och avbildningsmetoder.

ABSTRACT

Primary hyperparathyroidism (pHPT) is caused by one or more hyperfunctional parathyroid gland causing an inappropriately high release of parathyroid hormone (PTH) in relation to the calcium concentration in the blood. PTH acts on the bones to release more calcium and on the kidneys to reabsorb calcium, causing hypercalcemia. Approximately 75% of the patients are women and median age is 62. The only permanent cure is surgical removal of all pathologic parathyroid glands. To minimise the surgical exploration preoperative imaging localisation methods, have for decades been used and refined to pinpoint the culprit gland(s). The performance data for different imaging modalities used for preoperative localisation of hyperfunctional parathyroid glands are difficult to interpret. There are large numbers of studies on different methods with varying protocols and quality, often with insufficient reporting on important influencing factors such as adenoma weight and frequency of multiglandular disease (MGD). In this thesis we have analysed the performance of dual time-point ^{99m}Tc-sestamibi SPECT/CT for preoperative localisation of PTAs with regards to its individual components: ^{99m}Tc-sestamibi SPECT alone [S], nonenhanced CT (native phase) [N], contrast-enhanced CT (arterial- and venous phase), [A] and [V] respectively and in combination [AN], [VN], [SN], [ANS], [VNS] and [SNAV]. Additionally, the impact of the adenoma weight and MGD on PTA localisation was also investigated.

In ***Study I*** we retrospectively analysed 249 patients examined with nonenhanced ^{99m}Tc-sestamibi SPECT/CT and found that adding a diagnostic native phase to ^{99m}Tc-sestamibi SPECT significantly increased the localisation specificity from 93.5% to 95.9% ($p<0.01$), but not the sensitivity. In a prospective examination of 192 patients (***Study II***) we reported that adding an arterial and venous phase to nonenhanced SPECT/CT [SN] significantly increased the localisation sensitivity from 81.1% to 89.9% ($p<0.01$) without changing the specificity. Using the same cohort, in ***Study III*** we showed that adding ^{99m}Tc-sestamibi SPECT to different combinations of CT phases increased sensitivity e.g., 80.8% for [AN] as compared to 86.5% for [ANS] ($p<0.01$). However, the use of both contrast-enhanced phases was found redundant in terms of sensitivity gain, just adding 4 extra mSv.

The specificity was 97.9% for both. Although small parathyroid adenomas are known to be a challenge in preoperative localisation, we showed that it could be overcome using [ANS] or [SNAV]. The performance in patients with MGD remained unsatisfactory for all image sets, with a per-patient sensitivity of merely 30-40%. As a way of mitigating the consequences of this, in ***Study IV*** we trained a Machine Learning Classifier to recognise cases were preoperative localisation misclassified patients with MDG as single gland disease (SGD). As predictors, we used a set of pHPT related biochemical variables and the measured adenoma weight on patients cured after parathyroidectomy. On test data, the current classifier reached a 72% true positive prediction rate for MGD-patients and a misclassification rate of 6% for SGD-patients. These results call for further exploration before clinical implementation.

LIST OF SCIENTIFIC PAPERS

I. SPECT/CT's Advantage for Preoperative Localization of Small Parathyroid Adenomas in Primary Hyperparathyroidism
Patricia Sandqvist, Inga-Lena Nilsson, Per Grybäck, Alejandro Sanchez-Crespo and Anders Sundin
Clin Nucl Med. 2017 Feb;42(2):e109-e114.

II. Multiphase Iodine Contrast-Enhanced SPECT/CT Outperforms Nonenhanced SPECT/CT for Preoperative Localization of Small Parathyroid Adenomas
Patricia Sandqvist, Inga-Lena Nilsson, Per Grybäck, Alejandro Sanchez-Crespo and Anders Sundin
Clin Nucl Med. 2019 Dec;44(12):929-935.

III. The preoperative localisation of small parathyroid adenomas improves when adding Tc-99m-Sestamibi SPECT to multiphase contrast-enhanced CT
Patricia Sandqvist, Jacob Farnebo, Inga-Lena Nilsson, Per Grybäck, Anders Sundin, Alejandro Sanchez-Crespo
Insights Imaging. 2021 Jun 5;12(1):72.

IV. Primary hyperparathyroidism, a machine learning approach to identify multiglandular disease in patients with a single adenoma found at preoperative Sestamibi-SPECT/CT
Patricia Sandqvist, Inga-Lena Nilsson, Per Grybäck, Anders Sundin, Alejandro Sanchez-Crespo
Submitted to European Journal Endocrinology mars 2022.

ARTICLES NOT INCLUDED IN THE THESIS

Holstensson M, Smedby O, Poludniowski G, Sanches Crespo A, Savitcheva I, Oberg M, Gryback P, Gabrielson S, **Sandqvist P**, Bartholdson E and Axelsson R. Comparison of acquisition protocols for ventilation/perfusion SPECT - a Monte Carlo study. Physics in medicine and biology. 2019;64(23):235018.

Foukakis T, Lovrot J, **Sandqvist P**, Xie H, Lindstrom LS, Giorgetti C, et al. Gene expression profiling of sequential metastatic biopsies for biomarker discovery in breast cancer. Mol Oncol. 2015;9(7):1384-91.

Ardenfors O, Svanholm U, Jacobsson H, **Sandqvist P**, Gryback P, Jonsson C. Reduced acquisition times in whole body bone scintigraphy using a noise-reducing Pixon(R)-algorithm-a qualitative evaluation study. EJNMMI Res. 2015;5(1):48.

Larsson P, Arvidsson D, Bjornstedt M, Isaksson B, Jersenius U, Motarjemi H, et al. Adding 11C-acetate to 18F-FDG at PET Examination Has an Incremental Value in the Diagnosis of Hepatocellular Carcinoma. Mol Imaging Radionucl Ther. 2012;21(1):6-12.

Jacobsson H, **Larsson P**, Jonsson C, Jussing E, Gryback P. Normal uptake of 68Ga-DOTA-TOC by the pancreas uncinate process mimicking malignancy at somatostatin receptor PET. Clinical nuclear medicine. 2012;37(4):362-5.

Larsson P, Holzgraefe B, Kalzen H, Donnelly M, Porwit A, Jacobsson H. PET/CT examination in an anaplastic malignant lymphoma with extensive reactive involvement. Clinical nuclear medicine. 2008;33(9):619-20.

CONTENTS

LIST OF ABBREVIATIONS

4D-CT	Four-dimensional CT
BNE	Bilateral neck exploration
CECT	Iodine contrast-enhanced CT
CT	Computed tomography
CS	Confidence score
EF	Evaluation form
FHH	Familial hypocalciuric hypercalcemia
HU	Hounsfield units (CT-attenuation measure)
ioPTH	Intraoperative parathyroid hormone
kV	kilo Voltage
LDCT	Low-dose CT
mAs	milli Ampere second
MGD	Multiglandular disease
MIP	Minimally invasive parathyroidectomy
MLC	Machine learning classifier
MRI	Magnetic resonance imaging
NECT	Non-contrast-enhanced CT
OSEM	Ordered subset expectation maximisation
PET	Positron emission tomography
pHPT	Primary hyperparathyroidism
PTA	Parathyroid adenoma
PTH	Parathyroid hormone
SGD	Single gland disease
SPECT	Single photon emission computed tomography
^{99m}Tc	Metastable nuclear isomer of the element technetium-99
UNE	Unilateral neck exploration
US	Ultrasonography
[S]	^{99m}Tc-sestamibi SPECT alone image set
[N]	Native phase CT image set
[A]	Arterial phase CT image set

[V]	Venous phase CT image set
[XYZ]	Image set combined of [X]+[Y]+[Z]

1 INTRODUCTION

1.1 PRIMARY HYPERPARATHYROIDISM

1.1.1 Definition

Primary hyperparathyroidism (pHPT) is a common endocrine disease caused by hyper-secretion of parathyroid hormone (PTH), affecting the calcium-homeostasis by acting on the bone, kidneys and indirectly, by activation of vitamin D, on the intestine to increase the calcium level in blood. It is characterised by hypercalcemia and elevated or inappropriately normal PTH in relation to the level of serum calcium (2, 3).

The cause of excessive PTH-synthesis is typically a single parathyroid adenoma (PTA). In a large meta-analysis of over 20 000 patients, the parathyroid pathology was distributed as follows: A single adenoma accounted for 89%, multiple parathyroid gland hyperplasia 6%, double adenomas 4% and parathyroid carcinoma for less than 1% (4). However, according to a recently updated WHO classification (2022) of parathyroid tumours, hyperplasia is now considered primarily a part of secondary hyperparathyroidism and the affected glands of multiglandular disease in primary hyperparathyroidism are instead regarded as "multiple neoplastic proliferations" (5).

In secondary forms of hyperparathyroidism, various conditions (renal failure, vitamin D deficiency, malabsorption), causing hypocalcemia results is an appropriate response of the parathyroid glands causing elevation of PTH to counteract the hypocalcemia. Some drugs (lithium, thiazide-diuretics and bisphosphonates) may also cause pathological elevation of PTH (6).

1.1.2 Etiology

Sporadic: More than 90% of pHPT is sporadic and the cause is usually unknown. Irradiation of the neck in young age and long-term lithium treatment might be risk factors and account for a small number of cases (7). The famous cohort of nurses in the Nurses' Health Study has been analysed regarding connection between lack of physical activity and hyperparathyroidism. They concluded that low physical activity may be a modifiable risk factor for pHPT (8).

Familial: Up to 10% of the patients may be part of hereditary endocrine syndromes like Multiple Endocrine Neoplasia (MEN1, MEN2A), Hyperparathyroidism-Jaw Tumour (HPT-JT), Familial isolated hyperparathyroidism (FIHPT) and Familial Hypocalciuric Hypercalcemia (FHH) (7).

1.1.3 Epidemiology

The true incidence of pHPT is hard to establish, due to its common asymptomatic form. Before the era of multichannel biochemical screening, evolving in the 1970s, pHPT was considered a rare disease that usually presented with overt symptoms. When the calcium

concentrations in the blood could easily be analysed, the incidence raised 4-5-fold (2, 3, 9) and many of these patients were asymptomatic, or had only mild disease, but were at risk of developing symptomatic disease over time. The screening of osteoporosis in postmenopausal women, that started in the end of the 1990s, could have been a contributing factor to the later discovered increase in pHPT incidence in the western world (2).

The current geographical differences in incidence are largely depending on the presence or absence of biochemical screening (10). An American study (11) indicated a mean (all age-groups) incidence of 66 per 100 000 person-years among women and 25 among men, but as high as 196 and 95 for women and men aged 70-79 years, respectively. In a Danish report (12) the incidence was 16 per 100 000 person-years. Incidence increases markedly with age (11, 12) and especially in postmenopausal women.

1.1.4 Diagnosis

Primary hyperparathyroidism is diagnosed based upon biochemical testing to differentiate the condition from secondary forms of HPT and other causes of hypercalcemia (malignancy, granulomatous diseases), for which the aberration is not primarily located in the parathyroid glands (2, 3).

It is also necessary to rule out FHH, a condition mimicking mild pHPT, but without any serious negative consequences and no need for surgery. FHH is caused by a genetic aberration in the calcium sensing receptor (CaSR) making it less sensitive to the calcium-concentration and resulting in less negative feedback of the PTH-synthesis in the parathyroid cells and less excretion of calcium by the kidneys to the urine (7).

Biochemical evaluation: Albumin-corrected p-calcium and / or ionised s-calcium, p-PTH, p-phosphate, p-creatinine, vitamin D (25-hydroxyvitamin D), 24h u-calcium, 24h u-creatinine (2, 3).

Evaluation of complications: (3)

Dual-energy X-ray Absorptiometry (DXA) for measurement of bone mineral density in osteoporosis screening.

Spine X-ray in suspicion of vertebral compression fracture (pain, loss of height).

1.1.5 Symptoms

In the western world, the disease is often incidentally discovered due to biochemical aberrations and the patient may be asymptomatic. In other parts of the world with less developed healthcare systems (less use of biochemical screening) the disease is usually detected as a consequence of symptoms, hence symptomatic disease is common (3).

Symptomatic pHPT

Skeletal pain and fractures due to osteoporosis or even osteitis fibrosa cystica, sometimes occur, induced by increased osteoclast activity. Increased load of calcium on the kidneys may cause nephrolithiasis and nephrocalcinosis with risk of developing renal failure. Abdominal pain may be present, originating from renal stone disease, pancreatitis, gastric ulcers and obstipation. Other features are proximal muscle weakness, fatigue, cognitive impairment and depression. The disease is associated with increased risk of cardiovascular involvement, such as hypertension and cardiovascular mortality (2, 3).

Asymptomatic pHPT

The condition is defined by biochemically established pHPT without any overt symptoms or target organ manifestations (skeletal or renal). Today this form of disease accounts for roughly 80% of the patients in the western world. The natural history of asymptomatic pHPT varies. Some patients may remain stable in terms of bone density and renal function while as many as 40% deteriorate within 15 years of follow up (3).

1.1.6 Embryology and anatomy

Due to complicated embryology, including migration and split buds, the anatomy of the parathyroid glands is highly variable. This is obviously important in parathyroid surgery and one of the main reasons for preoperative parathyroid imaging. There are usually four parathyroid glands, although their numbers can vary. Studies from autopsies have shown four glands in 84-93 %, 5 or more in 5-13 % and 3 or less glands in 2-3% (13, 14). Normal parathyroid glands at autopsy-study measured 1 x 4 x 7 mm and weighed 30-60 (mean 40) mg (13).

There is usually one upper and one lower pair of parathyroid glands. The upper pair (sometimes referred to as P4) originates from the 4th brachial arch, and the lower pair from (P3) from the 3rd brachial arch. The final location of the upper pair glands are normally behind the upper half of each thyroid lobe (80%) and the lower pair in close proximity to the lower pole of each thyroid lobe (50%) (15). The respective frequency of their different potential anatomical positions is illustrated in **Figure 1.1**. Parathyroid glands in an atypical position are defined as ectopic, and those in an ordinary location are sometimes referred to as eutopic. Since the lower pair has a more cranial origin and a longer migration to its final more caudal destination, these glands are more prone to vary in location than the upper ones.

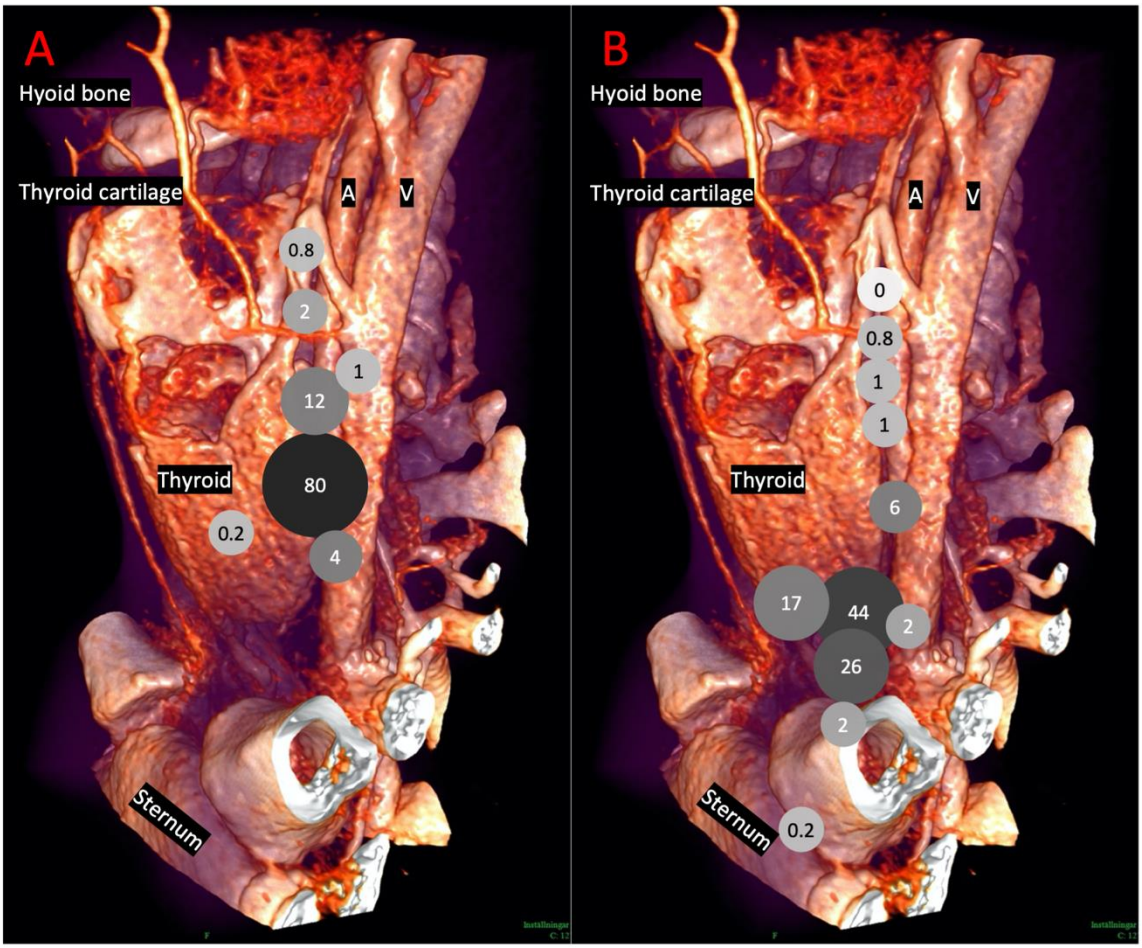

***Figure 1.1**. Localisation distribution (%) of eutopic and ectopic location of upper parathyroid glands (P4) **(A)** and for lower parathyroid glands (P3) **(B)**. This distribution was found by Åkerström et al. (16), but has been applied by us in these 3D volume rendering CT images of soft tissues in the neck from a patient in our second cohort.*

1.1.7 Treatment

Parathyroidectomy, with the removal of all pathological parathyroid glands, is the only known cure of primary hyperparathyroidism. It is recommended in all patients suffering from classical symptoms, provided the absence of contraindications. For asymptomatic patients, surgery is advisable too, when any of the below listed indications are met, according to several consensus meetings and guidelines (2, 17, 18).

Indications for surgery in asymptomatic patients according to an international workshop (18):

1. S-Ca >0.25 mmol/L above upper limit of normal
2. Bone mineral density (BMD) < -2.5 standard deviations (osteoporosis) at any of three locations: lumbal spine, hip or distal radius
3. Vertebral fracture on radiological examination
4. Creatinine clearance < 60 ml/min
5. 24 h urine Ca > 10 mmol/d
6. Nephrolithiasis or nephrocalcinosis (X-ray, CT or ultrasound)
7. Age < 50 year

For patients with non-classical symptoms, the indication for surgery is more controversial and it is still hard to predict the effect of surgery on an individual basis (6). Some emerging tools have however recently been reported (19, 20), such as calcimimetics a short period preoperatively to test for reversibility of symptoms.

The traditional way of performing parathyroid surgery used to be bilateral neck exploration (BNE), with the aim to identify and evaluate all four parathyroid glands for adenoma and hyperplasia. This procedure may vary, and in cases where all parathyroid glands do not have an eutopic location, extended neck dissection maybe needed, involving the carotid sheaths, the retroesophageal and the retropharyngeal space and thymectomy. Intrathyroidal and the rare intravagal localisation also need to be considered.

Improved imaging methods for preoperative localisation of pathological parathyroid glands have opened up for less extensive surgical techniques. In patients without obvious risk of MGD in whom preoperative imaging have clearly pinpointed a single enlarged parathyroid gland, a focused surgical approach is suitable. This can be performed as minimally invasive parathyroidectomy (MIP) with only a short incision enough to be able to excise the culprit gland. A variant of this is the unilateral neck exploration (UNE), where both the upper and lower parathyroid glands are explored on one side.

Patients with established hyperparathyroidism, as part of a familial syndrome or due to lithium-treatment, have a high frequency of MGD and should therefore in case of surgery undergo BNE (21). A subtotal parathyroidectomy, when only about the size of a nomal is spared, is usually employed in those cases (22). Sometimes the spared parathyroid tissue is auto-transplanted into the subcutaneous tissue on the volar side of the forearm or, in the brachio-radialis muscle (23). Some authors recommend a more conservative initial approach with removal of only abnormal parathyroids, or unilateral clearance for patients with concordant localising studies, to avoid the high risk of permanent hypoparathyroidism associated with subtotal parathyroidectomy (24).

A way of predicting cure in the intraoperative setting is to measure PTH before and after removal of a pathologic parathyroid gland, using a so-called intraoperative parathyroid hormone (ioPTH) monitoring. Since PTH has a short half-life of 4 minutes, the PTH-level will decrease rapidly after removal of the pathologic parathyroid gland. A drop in PTH-level of 50% or more, within 10-15 minutes after the removal, is indicative for cure. If the PTH level remains high, MGD should be considered, or that something other than a parathyroid adenoma (PTA) has been removed.

There is some criticism claiming that the method is sometimes difficult to interpret, or falsely indicates remaining hyper-functioning parathyroid tissue. This may lead to unnecessary BNE and prolonged operation-time (25).

The overall frequency of ectopic PTAs varies in different reports: 10%, 8,5%, 22% (13, 26, 27), as well as the distribution among different ectopic locations: Thymus 30-40%,

retro/paraesophageal 25-30%, intrathyroidal 15-20%, mediastinum 6-14%, undescended 4%, carotid sheath 3% (27, 28). The mean adenoma weight have been shown to be similar in ectopic and eutopic glands (28).

A recent study has reported that the number of parathyroidectomies performed in Sweden during the decade (January 1, 2008 – December 2017) was 8626 (29). 77% were women. The annual number during this period, has remained stable at around 850, with only minor variations (30). Outpatient surgery (when the patient can return home the same day) is an emerging alternative (120 patients in 2016 and 341 in 2019) (31). The average age among those undergoing surgery 2018 was 62 years (32). Bilateral neck exploration has decreased from almost 70 % of procedures in 2005 to around 25 % in 2019 (32).

The cure-rate and the risk of complications in parathyroidectomy have been evaluated for various surgical approaches in a large meta-analysis including 9643 patients undergoing MIP and 2471 who underwent BNE, respectively. The cure rate was similar (97 vs. 98 %), as was the infection risk (0.5%). However, the risk of hypocalcemia (2.3 vs. 13.6 %) and laryngeal nerve palsy (0.3 vs. 0.9 %) was significantly lower with MIP than for BNE (33).

Another meta-study including 12743 patients also showed similar overall cure-rates for MIP and BNE, but significantly shorter operative time (mean difference almost 40 minutes) and lower risk of transient hypocalcemia for those who underwent MIP (34).

1.2 IMAGING FOR PREOPERATIVE LOCALISATION

1.2.1 General aspects

There is a broad consensus that the diagnosis hyperparathyroidism is established using biochemistry and that preoperative imaging should not be used as a diagnostic tool (22). The use of imaging should be reserved exclusively for patients with an established pHPT diagnosis and for whom there is surgical intention (35-37).

There are several motives for preoperative localisation. The guiding of the surgeon by imaging allows for focused surgical procedures, such as MIP and UNE. It is also important for locating ectopic PTAs, and prior to surgery in patients with persistent or recurrent disease. Imaging may also be used as an indicator when to perform BNE or include ioPTH measurement, when imaging is inconclusive and in cases of suspicious MGD. In patients where imaging has difficulty distinguishing between a PTA and a thyroid nodule or other entities, the same imaging can be used for guidance of a fine needle aspiration for further workup. In rare cases, imaging can also pick-up signs suggestive for parathyroid cancer which is essential for the surgical planning (38).

Since the start of preoperative imaging for the purpose of localisation of PTAs in the mid 50th, many methods have been developed, all with its pros and cons. Many have by now been

dethroned, but since no method has proven optimal for all patients and the field has been very dynamic, history has left us with a plethora of methods and examination protocols.

1.2.2 Major advances in locating parathyroid adenoma from a historical perspective

- *1954. Arterial angiogram*

One of the first to attempt (if not the first) to preoperatively localise PTAs using imaging techniques was the Swedish radiologist Sven Ivar Seldinger. He performed bilateral arteriograms injecting contrast media through a catheter positioned in the subclavian artery. By visualising displacement of the normal configuration of the inferior thyroid artery and its branches, he was able to predict the presence of soft tissue masses suspicious for a PTA in 4 out of 6 patients (**Figure 1.2**) (1).

Figure 1.2. *An arteriogram of the right and left subclavian artery and the thyreocervical truncs. The arrows indicate a displaced widened loop of a branch from the left inferior thyroid artery suggesting the presence a soft tissue mass (a PTA). This image was originally published in Acta Radiologica by Seldinger SI et al. (1).*

- *1965.* ^{75}*Se-Selenomethionine*

Potchen reported on preoperative localisation using the γ-emitting amino acid analogue ^{75}Se-selenomethionine. External detection was performed using a Picker Magnascanner with 5-inch thallium-activated NaI crystal. Good correlation between scan and surgery was shown in 11 out of 16 patients (39).

- *1969. Selective venous sampling*

In the 60th the development of the radioimmunoassay technique made it possible to measure the concentration of PTH in blood. Reitz et al., in the end of that decade, applied this technique in combination with selective venous catheterisation to measure the PTH-levels in the veins draining each side of the neck and thorax, serving as guidance to locate PTAs (40).

- *1975. Ultrasonography*

Arima et al. used ultrasonography for localisation of parathyroid tumours in ten patients, with success in seven of those (41).

- *1975. Radionuclide subtraction of thyroid activity*

Ell et al. developed the first radionuclide subtraction method for localisation of PTAs, using the established ^{75}Se-selenomethionine scan with the novelty of computer aided scaled subtraction of the thyroid uptake from a ^{125}I-sodium iodine scan (42).

- *1977. Computed tomography (CT)*

Doppman et al. were pioneers in using CT for localisation of PTAs. CT was reported useful for locating large occult PTAs in the mediastinum in patients with unsuccessful neck surgery, but disappointingly the performance of the equipment at that time (slice thickness of 15 mm) failed as a non-invasive routine method of localising PTAs in general (43).

- *1979. ^{201}Tl-chloride scintigraphy*

Fukunaga et al. found in one case accumulation of ^{201}Tl-thallous chloride in a PTA (44).

- *1983. PTH measurement in aspirates from suspected PTAs*

PTH immunoassay on CT- or ultrasonography-guided aspirations from suspicious parathyroid lesions was introduced by Doppman et al. High PTH content in a lesion was highly specific for parathyroid tissue (45).

- *1984. MRI*

The first report of using MRI for localisation of PTAs was presented by Stark et al. (46).

- *1988. Intraoperative measurement of PTH*

Brasier et al. analysed the kinetics of PTH in vivo after parathyroidectomy and found an exponential decay with a half-life of 21 minutes (47). Nussbaum et al., from the same institution, later that year reported that intraoperative measurement of PTH had the potential of guiding the surgeon to know when cure had been achieved (48).

- *1989. ^{99m}Tc-sestamibi scintigraphy*

A new radiopharmaceutical, ^{99m}Tc-sestamibi, initially used for myocardial studies (similarly to ^{201}Tl-chloride) was by Coakley et al. proven to be useful for localisation of PTAs. It had the advantage of higher parathyroid to thyroid uptake ratio, superior physical characteristics for the gamma camera detector and by far less radiation dose to the patient compared to ^{201}Tl-chloride (49).

- *1992. Dual time-point ^{99m}Tc-sestamibi scintigraphy*

Taillefer et al. presented an alternative to the prevailing dual tracer subtraction method, using instead a single tracer dual time-point regime with ^{99m}Tc-sestamibi scans at 15 min and approximately 2 hours after injection. The slower washout of the radiotracer from the

parathyroid than the thyroid usually makes it appear clearly in the late scan (**Figure 1.3**). The convenience of using one tracer only and avoiding the difficulties of postprocessing images greatly simplified the procedure (50).

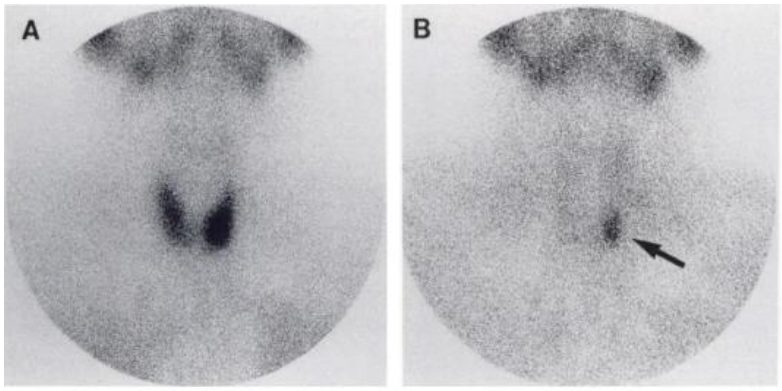

Figure 1.3. *^{99m}Tc-sestamibi parathyroid planar imaging at 15 minutes post administration (A) and approximately 2 hours post administration (B). This image was originally published in JNM by Taillefer R et al. (50).*

- *1993. ^{18}F-FDG Positron Emission Tomography (PET)*

Neumann et al. published a report on a case of a localised PTA using ^{18}F-fluorodeoxyglucose (FDG).

- *1994. ^{11}C-methionine PET*

Hellman et al. revived methionine as a tracer for localisation of PTAs, but replaced the previously used gamma-emitting radionuclide ^{75}Se with the positron-emitting radionuclide ^{11}C to use PET for localisation (51).

- *1995. Intraoperative gamma radiation probe*

Martinez et al. demonstrated that a portable γ-radiation detecting probe could facilitate localisation in the intraoperative setting 2-6 hours after administration of ^{99m}Tc-sestamibi (52).

- *2003. SPECT/CT*

The first report of a hybrid imaging study for localisation of PTAs was published in 2003. Kaczirek et al. performed in four patients a ^{99m}Tc-sestamibi SPECT/X-ray-CT using a gamma camera equipped with an X-ray tube and X-ray detectors (Hawkeye system from GE) (53). The advantage of this new imaging system was mainly the better perception of the anatomical localisation.

- *2006. 4-Dimensional Computed Tomography (4D-CT)*

Another study in the field that has attracted a lot of attention was presented by Rodgers et al. They reported that 4-dimensional CT (4D-CT), a 3-dimensional CT scanning with an added 4th dimension, in terms of the dynamic changes of contrast enhancement over time (precontrast, postcontrast (25 s) and "delayed scan"), in a single examination session offered assessment of both anatomy and perfusion (54).

- *2012. ^{11}C-choline 2013. ^{18}F-fluorocholine PET/CT*

Two incidental findings of focal uptake in the neck, using choline PET/CT in patients staged for prostate cancer, was found by Mapelli et al. 2012 (55) and Quak et al. 2013 (56) using ^{11}C-choline and ^{18}F-fluorocholine respectively. Both were found to correspond to PTAs. Subsequently Lezaic et al. followed up by conducting a study confirming the feasibility of using ^{18}F-fluorocholine PET/CT and presented remarkable results with 92% sensitivity (57).

1.2.3 The uptake mechanism of ^{99m}Tc-sestamibi

Sestamibi is a lipophilic cationic complex. Its lipophilic property allows it to diffuse through the plasma membranes of the cells and the mitochondria. The positive charge of sestamibi causes it to diffuse along the electrochemical gradient attracted by the negative charge induced inside active mitochondria (**Figure 1.4**). It is the richness of active mitochondria predominantly in the oxyphil cells of hyperfunctioning parathyroid glands that make them accumulate sestamibi to a lager extent than other tissues (58).

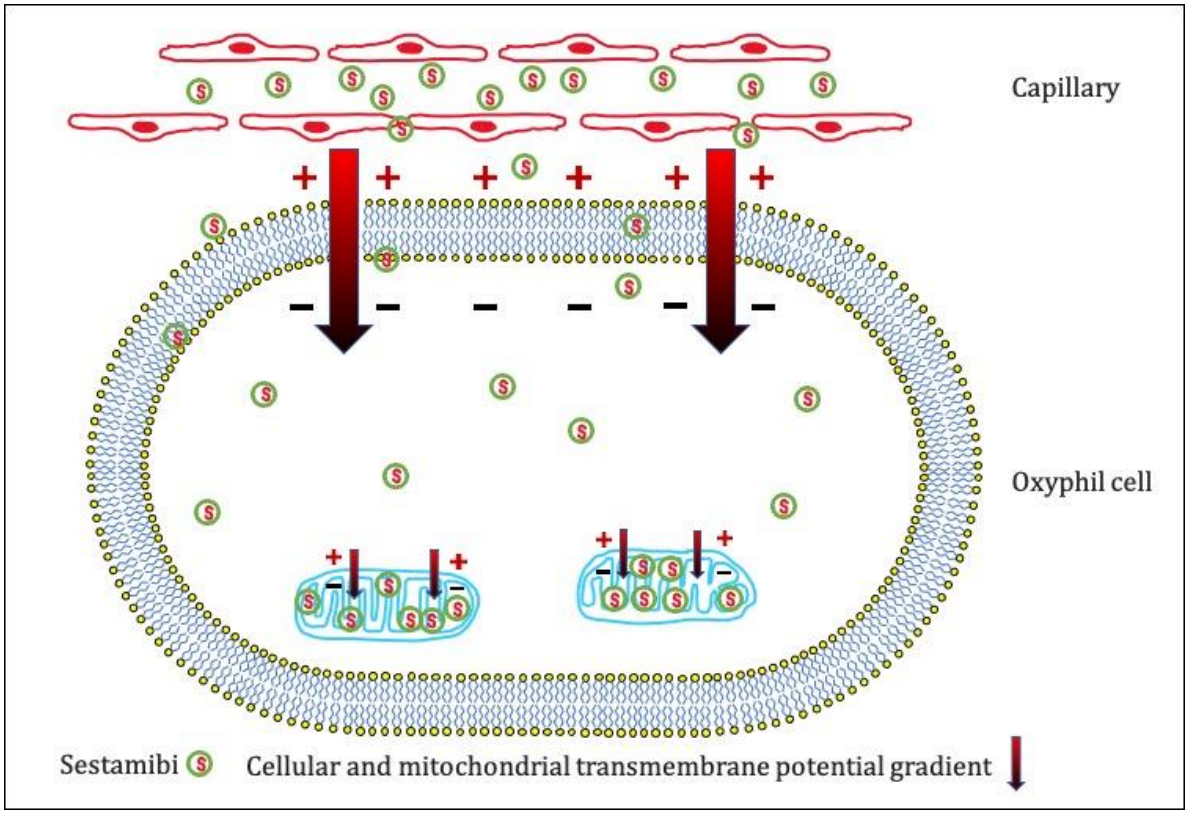

***Figure 1.4**. The diffusion of sestamibi from the blood-pool into the many active mitochondria in oxyphil cells of a hyperfunctioning parathyroid gland.*

1.2.4 Partial volume effects in gamma camera imaging

In gamma camera imaging there is a trade-off between spatial resolution and camera sensitivity. The major contributors to this trade-off are the collimator and the scintillator crystal. A collimator is necessary to ensure absorption of obliquely incident photons in

relation to the scintillator crystal. Theoretically, only perpendicularly incident photons should be used to form an image. Hence, the collimator is required to achieve a certain spatial resolution, but to the cost of reducing sensitivity. Different collimator types (hole diameter and lamella thickness) result in different gamma camera sensitivity and spatial resolution. In a gamma camera, the scintillator crystal is required to transform the incident photons into a signal. Thicker crystals have higher photon absorption, resulting in increased detection sensitivity but at the cost of an increased absorption of photons scattered within the crystal, reducing spatial resolution. While the collimator can be changed in accordance with the specific photon energy of the used radionuclide, the scintillator crystal is fixed. Hence, the overall gamma camera spatial resolution is a result of the combined physical characteristics of the collimator-crystal pair and is represented by a gaussian function (system point spread function (PSF)). The gamma camera resolution is characterised by the full width at half-maximum (FWHM) of the PSF. For a plane parallel-hole collimator, the PSF is broadened with increasing source-collimator distance. In SPECT the used image reconstruction algorithm and noise filters further reduces the image spatial resolution. In clinical practise, this limited spatial resolution results in the so-called partial volume effects (PVE). The PVE influences the ability to image activity distributions smaller than the FWHM of the overall PSF. This effect is even stronger in the presence of a background activity (spill in effect). As **Figure 1.5** shows, the net effect of the limited spatial resolution in gamma camera imaging on object detectability depends on both the object size in relation to gamma camera resolution and on the level of activity in the object in relation to the background. Since hyperfunctioning parathyroid glands are usually small structures, a delicate balance between spatial resolution and sensitivity is fundamental for their localisation. The normal anatomical localisation of the PTA, in the proximity to the thyroid, constitutes another challenge, since the thyroid also accumulates ^{99m}Tc-sestamibi.

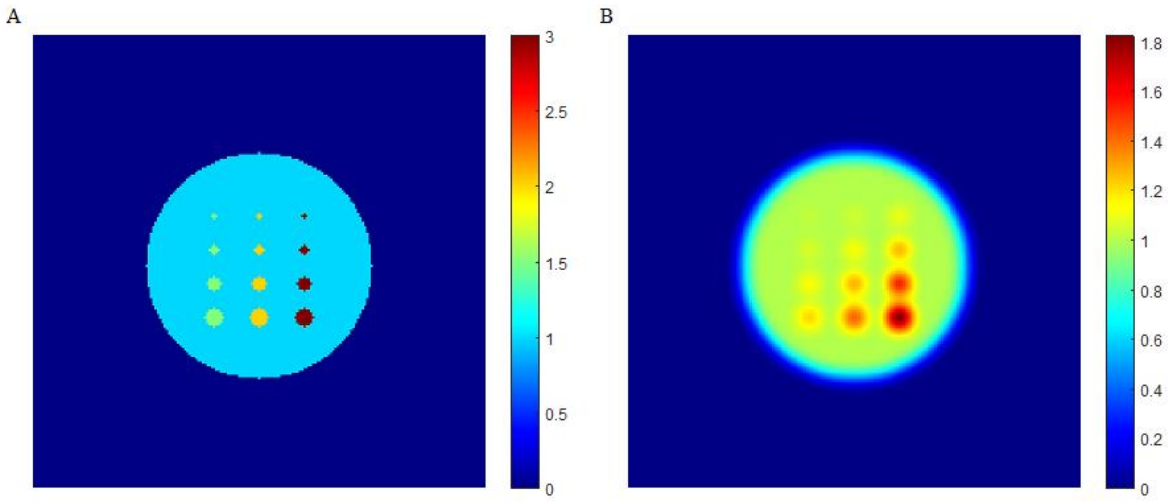

Figure 1.5. *(A) Simulated cylindrical phantom with 50 pixels radius and pixel intensity of 1 with inserted spheres of radiuses of 1, 2, 3 and 4 pixels. The activity distribution (pixel intensity) within the small spheres were,1.5, 2 and 3, respectively. (B) Simulated gamma camera projection of the phantom using a point spread function with 10 pixels full width at half-maximum point spread function.*

1.2.5 Common clinical practice of today

Since no modality have proven optimal for PTA localisation, preoperative imaging has been, and still is, like solving a jigsaw-puzzle, piece by piece. Ultrasound and ^{99m}Tc-sestamibi scintigraphy have for long been the mainstays for preoperative localisation in most clinics and considered first-line methods (**Figure 1.6**). In case of inconclusive localisation using these modalities, a step up to second-line methods may be taken, especially in patients with persistent or recurrent disease. Development of multimodality (hybrid) imaging methods (SPECT/CT and PET/CT) have simplified the addition of more pieces to this puzzle. Many factors, besides the localisation performance of each method, affect the clinical practice. Access to the more advanced methods e.g., PET/CT, is limited mainly to some university hospitals, and is not available in many parts of the world. Also, there is usually a lack of capacity for imaging of large patient groups, because cancer patients' access to PET/CT is a priority.

Local tradition with experience of a certain regime is also important for the choice of imaging. This is especially true for ^{99m}Tc-sestamibi scintigraphy for which many different examination protocols exist, such as planar imaging with or without subtraction, SPECT alone, SPECT/CT with or without diagnostic CT, and with or without administration of iodine contrast media. Some modalities, like PET/CT, are way more expensive than others. Selective venous sampling (SVS) has, due to its invasive properties, been reserved mostly for localisation when other imaging has failed or been inconclusive, and prior to reoperation.

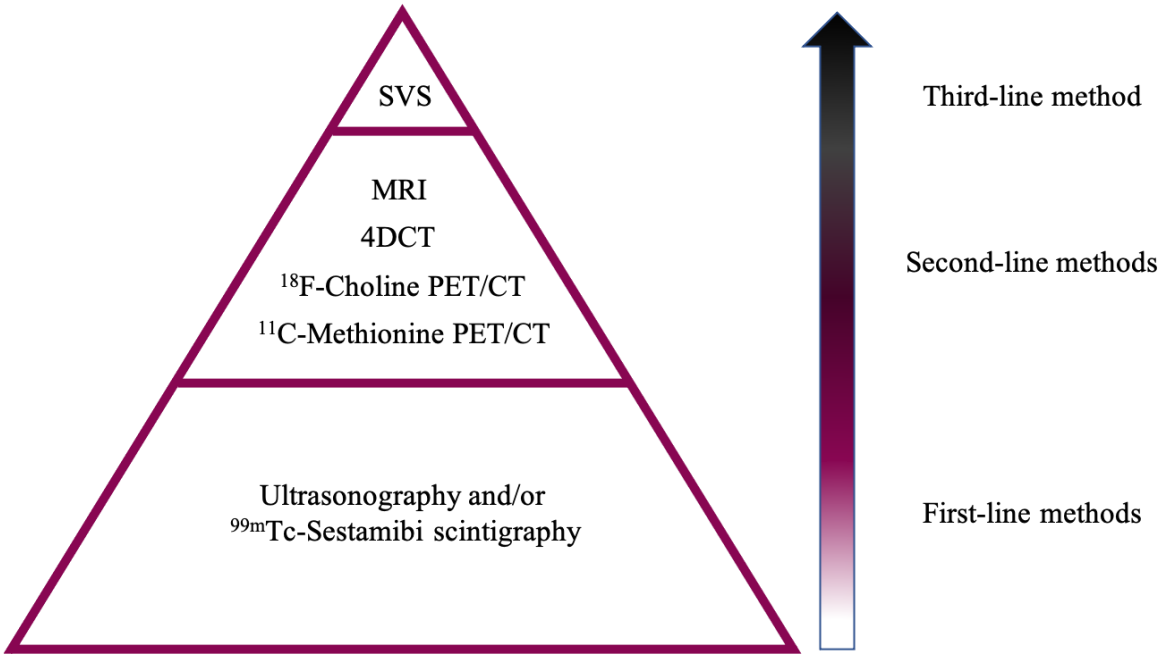

***Figure 1.6**. Image modalities for preoperative localisation of PTA and their status in common clinical practice. Their status is not fixed but under ongoing debate.*

1.2.6 Some well-known factors with negative impact on image localisation performance

There are many factors affecting the imaging performance, some true for all modalities and others more modality specific. Some review articles try to summarise strengths and weaknesses of different modalities, but much of the accumulated knowledge is empirical rather than scientifical (35). Some authors have performed multivariate logistic regression and other statistical analyses to investigate clinical and biochemical factors affecting the performance, but almost exclusively regarding ^{99m}Tc-sestamibi SPECT (59-64), except one analysis on 4D-CT (65). Low adenoma weight (small size), low calcium and phosphorous concentration and MGD all seem well established risk factors for negative imaging. Auto immune thyroiditis and cystic adenoma components might also affect imaging performance negatively, while age, gender, PTH and vitamin D insufficiency do not.
Below are some visual examples of factors complicating localisation, as illustrated with ^{99m}Tc-sestamibi SPECT/CT-images from our own ***Study II***, but many of these difficulties would be relevant also to other imaging modalities.

The size of PTAs (**Figure 1.7**) has an impact on the detectability (65) and non-localised pathological glands have been shown to be smaller and have lower weight (66).

A particular challenge in preoperative imaging is the detection of hyperfunctioning hyperplastic parathyroid glands in MGD (**Figure 1.8**) (35, 64, 66). MGD should be considered in patients with more than one enlarged gland on preoperative imaging (17). Although it may seem contradictory, negative imaging is also associated with higher frequency of MGD (64, 66). One reason for the imaging problems in MGD is probably the smaller size of PTAs compared to those of single gland disease (SGD) (67). This is however not the sole explanation, at least not concerning ^{99m}Tc-sestamibi scintigraphy, since the lower imaging sensitivity in MGD, compared to SGD, remains even for weight matched adenomas (67). There are attempts to predict MGD by using scoring systems based on CT-findings (largest diameter, number of candidate lesions) and a so-called Wisconsin-score (a product of the level of S-Calcium and S-PTH) (68).

Another challenge is goitre (**Figure 1.9**). Enlargement of the thyroid gland, especially with extensive nodular elements, can displace the parathyroid glands and completely obscure the presence of a PTA or, even worse, simulate one. Two studies have reported the advantage of SPECT/CT compared to SPECT alone, for preoperative localisation of PTA in patients with goitre (69, 70).

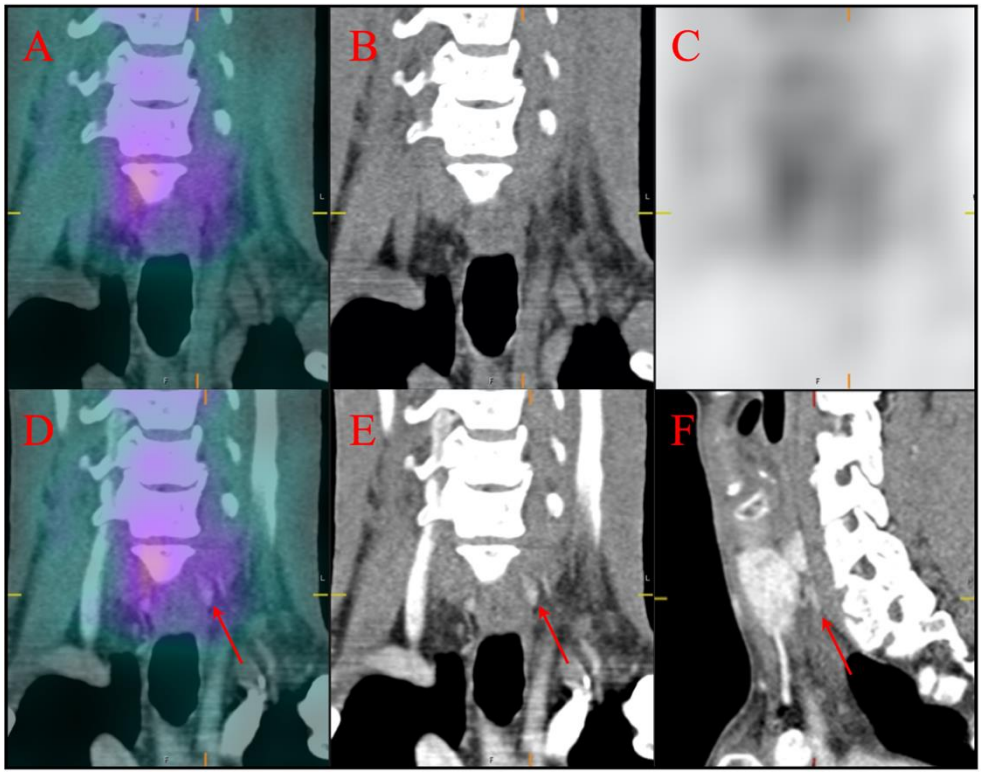

***Figure 1.7**. A small paraesophageal PTA with iso-attenuating surroundings in the native phase (B) and with no detectable sestamibi uptake (C). Only the arterial phase contributes to the detection (red arrow) (E and F).*

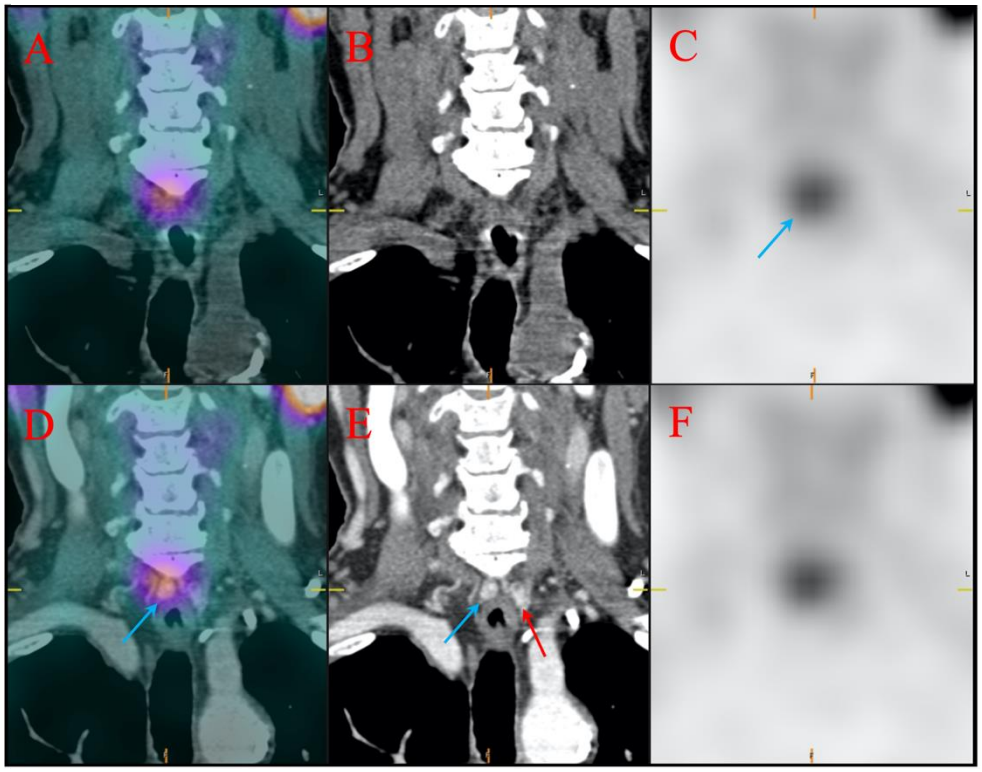

***Figure 1.8**. A patient with MGD with one paraesophageal PTA on each side. Only one focal sestamibi uptake can be discriminated (blue arrow in C and D). However, on contrast-enhanced CT images two enhancing soft tissue nodules are found (blue and red arrow in E), both corresponding to parathyroid adenomas. The non-enhanced phase (B) does not contribute to detection.*

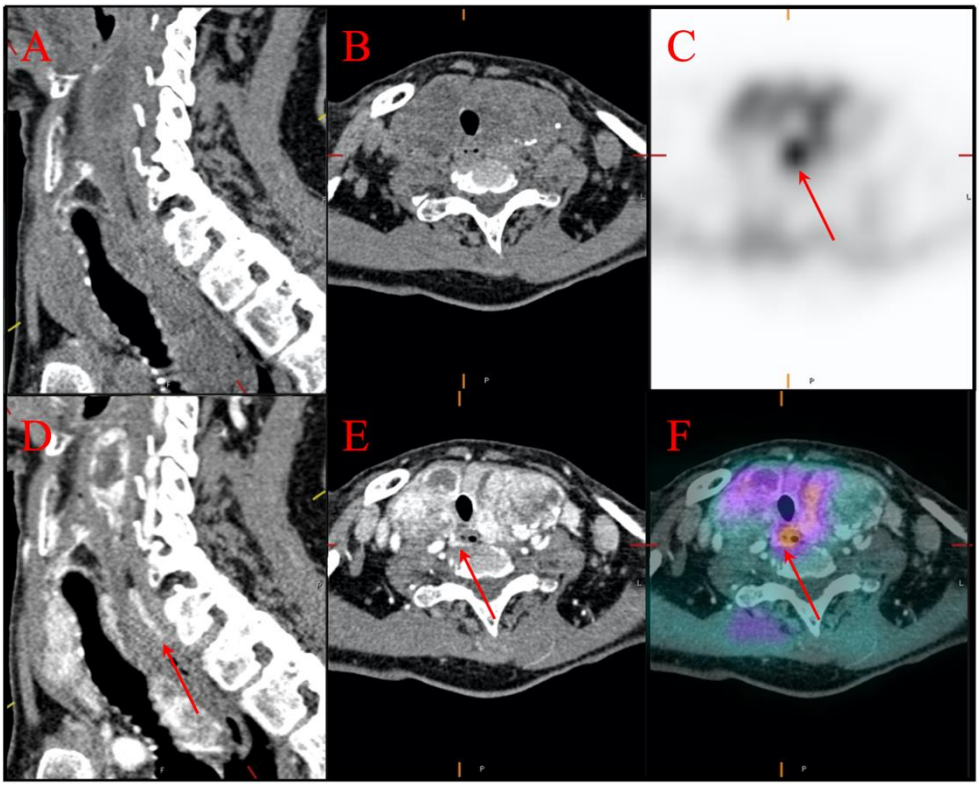

***Figure 1.9**. A bulky nodular goitre has compressed and displaced a parathyroid adenoma into the retroesophageal space to the right if the midline (red arrows). Two combined image features contribute to detection in this case: The focal sestamibi uptake (C and F) together with distinct contrast enhancement of a corresponding soft tissue nodule (D, E and F). The native phase does not contribute (A and B).*

The thyroid gland through a physiological process actively accumulates iodine for thyroid hormone synthesis. It has been demonstrated that there is a positive correlation between the CT-attenuation of the thyroid gland and its concentration of iodine (71). Several studies have shown a "natural" difference in the CT attenuation of the thyroid gland (higher) and that of PTAs (lower), on a non-contrast-enhanced CT (72, 73). However, this may change with pathological conditions of the thyroid, e.g., in patients with autoimmune thyroiditis. A decrease in attenuation (Hounsfield Units, HU) of the thyroid gland may, thus, appear in both hypo- and hyperthyroidism (74). This is illustrated in **Figure 1.10** in a patient, in whom the difference in attenuation between the thyroid and the PTA has diminished.

Parathyroid adenomas with intrathyroidal location (**Figure 1.11**) may also be difficult to detect. They are rare, 2-4% of all patients (27, 28), especially compared to the abundant thyroid nodules of different types, that may have similar imaging characteristics. However, in the absence of a PTA elsewhere, and in the presence of a ^{99m}Tc-sestamibi accumulating well-defined intrathyroidal lesion with homogeneous low attenuation in the native phase together with contrast enhancement in arterial phase, an intrathyroidal PTA is a plausible diagnosis. Intrathyroidal PTAs are difficult for the surgeons to discover without information from preoperative imaging. One study has described some typical US-features of intrathyroidal PTAs: Hypoechoic, well defined lesion with a hyperechoic rim, rich blood supply (on

Doppler) usually located in the middle or lower part of a thyroid lobe (80%). Calcifications that are common in thyroid lesions were not seen in the PTAs, although in one case of parathyroid cancer (75).

In cystic PTAs (**Figure 1.12**), many typical imaging features may be deranged, and sometimes they are hard to differentiate from cystic thyroid nodules. There are however some characteristics that could suggest a PTA: signs of separation from the thyroid, a solid contrast-enhancing and ^{99m}Tc-sestamibi accumulating component adjacent to the cystic wall.

Ectopic mediastinal localisation (**Figure 1.13**), except perhaps for those in the very upper part, is above all a surgical problem since the PTA is not visualised during operation, and in these instances preoperative imaging is crucial. Ectopic mediastinal localisation sometimes require sternotomy, which may need assistance of a thoracic surgeon. Because the mediastinum is covered by air-filled lungs and the sternum, the ultrasound does not work. The fact that mediastinal PTA location is rare (<1%) (27), and that mediastinal lymph nodes by contrast are very common, may cause an adenoma to be falsely interpreted as representing a lymph node. Other than that, there are usually fewer distracting elements in this location than in the cervical region. Other ectopic foci such PTAs within the carotid sheath or with intrathyroidal location, are usually more difficult to discern.

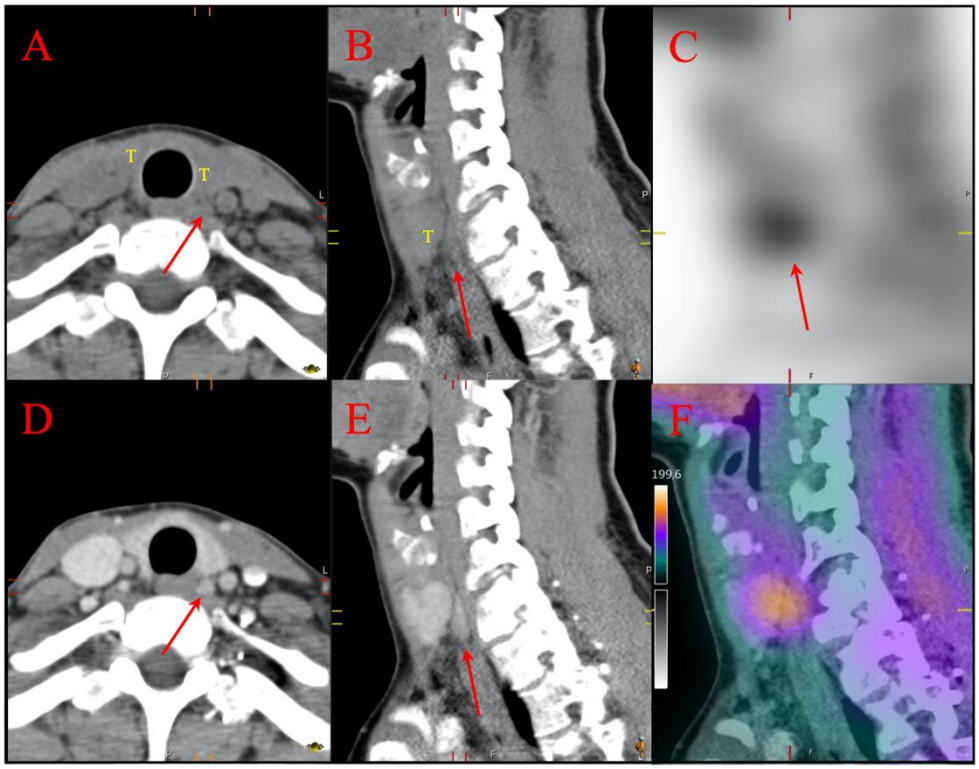

***Figure 1.10**. Low and similar attenuation in the thyroid gland (yellow T) and a parathyroid adenoma (red arrow), not clearly distinguishable in non-contrast enhanced CT (A and B). The parathyroid adenoma is detected mainly due to the distinct focal sestamibi uptake (C and F), but the contrast enhancement facilitates the outlining of a soft tissue nodule behind the thyroid (red arrow in D and E).*

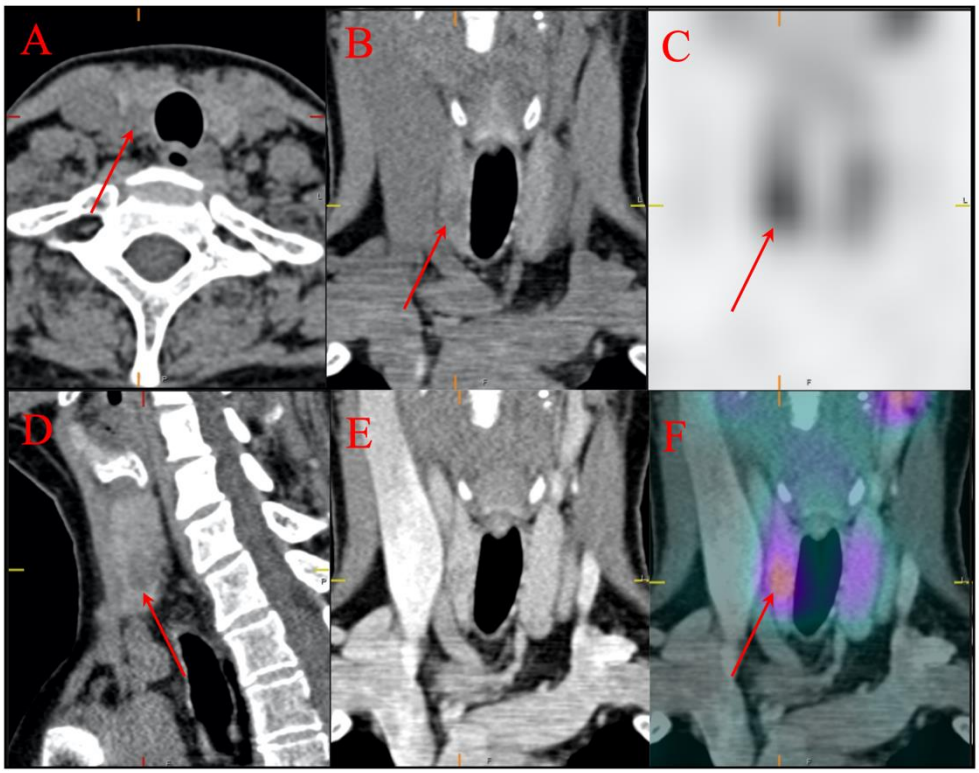

***Figure 1.11**. An intrathyroidal parathyroid adenoma located in the middle part of the right thyroid lobe (red arrow). In this patient the native phase (A, B and D) plays an important role since the "natural" higher attenuation of the thyroid gland, along with the focal sestamibi uptake (C and F) contribute to the detection. In the arterial phase (E) attenuation of the PTA is almost the same as in the thyroid gland.*

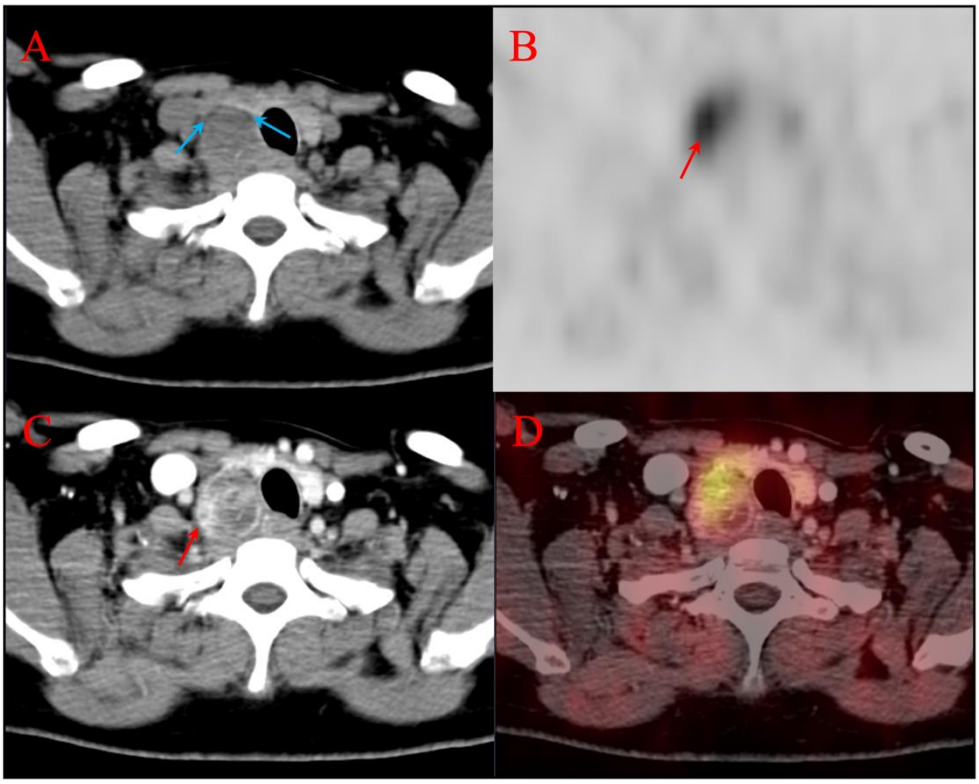

***Figure 1.12**. A cystic parathyroid adenoma separated from the thyroid gland by a thin layer of fat (blue arrows in A). The contrast-enhancing solid part (red arrow in C) also accumulates sestamibi (red arrow in B).*

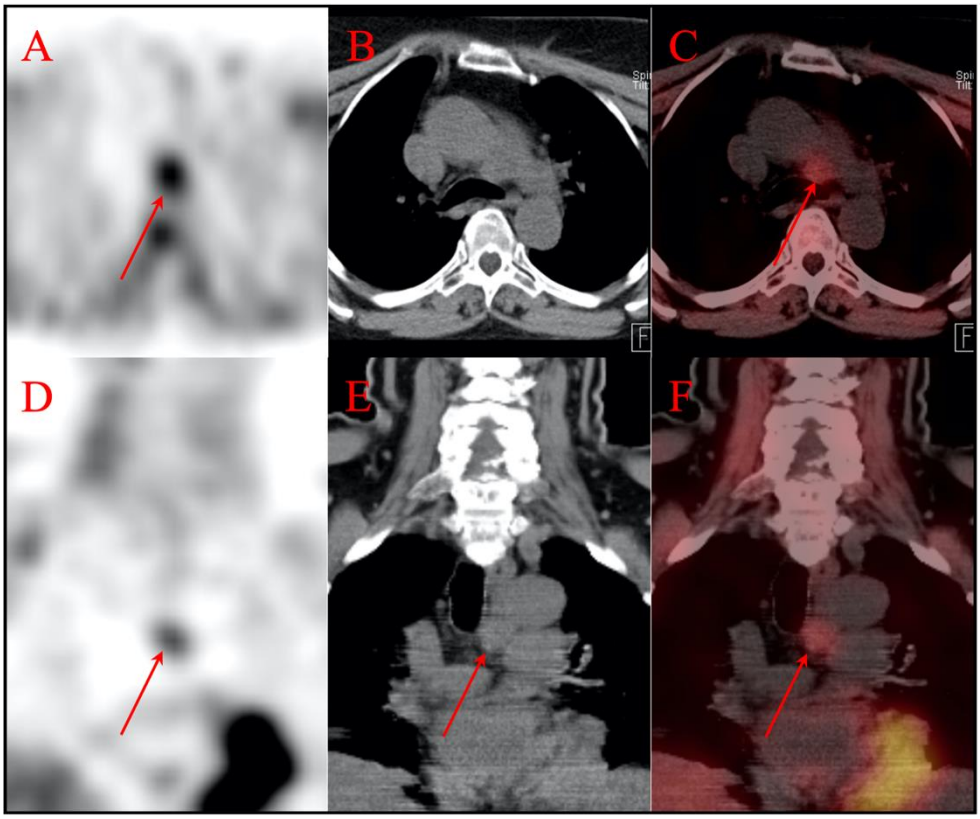

***Figure 1.13**. A mediastinal PTA (red arrow) with focal sestamibi uptake (A and D). Nonenhanced CT (B and E) does not contribute much to detection, but rather to elucidate the topographic anatomy.*

2 LITERATURE OVERVIEW

2.1 INTERNATIONAL GUIDELINES

There are several organisations that have issued both general and more focused recommendations regarding the management of primary hyperparathyroidism aimed at endocrine surgeons, endocrinologists, radiologists and nuclear medicine physicians.

- The European Association of Nuclear Medicine (EANM) practice guidelines for parathyroid imaging (37)
- American Head and Neck Society (AHNS) Endocrine Surgery Section - Update on parathyroid imaging (76)
- The American Association of Endocrine Surgeons (AAES) Guidelines for Definitive Management of Primary Hyperparathyroidism (77)
- A Canadian and international consensus (78)

These guidelines are, however, quite vague concerning the choice of preoperative imaging method.

The AHNS endocrine surgery section state in their conclusion that "Dependent upon availability, efficacy, and cost-effectiveness in a particular practice setting, high-definition neck ultrasound performed by those with experience in parathyroid ultrasonography, planar ^{99m}Tc-sestamibi imaging with SPECT or SPECT-CT, multiphase CT (2D, 3D, or 4D), and MRI may be reasonably used in conjunction"

The AAES have a strong recommendation that an experienced clinician should be involved in the decision of what image method to perform based on the regional resources and experience (77).

The Canadian and international consensus is not more precise in their statements "Ultrasound, 99mTc-sestamibi scintigraphy continue to be useful localisation tools, however, they can miss small adenomas and hyperplasia" and "Identification of abnormal parathyroid tissue is enhanced with single photon emission computed tomography (SPECT) study in combination with a computed tomography (CT) study and is particularly valuable in repeat surgical cases" (78).

The latest guidelines from EANM however, in the conclusion finally state that "the use of first-line imaging is important" and that "Sestamibi SPECT/CT and US is a widely available and accepted first-line strategy". ^{18}F-fluorocholine is also considered a potential "alternative" first-line modality (37).

On the other hand, there are some strong statements regarding the indication and the impact of preoperative localisation common in these guidelines:

1. Imaging must not be used for the diagnosis of pHPT (it is a biochemical diagnosis).
2. Indication for imaging arise only after decision to proceed with surgical treatment for pHPT.
3. Imaging offers guidance for operative planning (MIP, BNE, need for participation of a thoracic surgeon) by identifying the number and the anatomical location of hyperfunctioning parathyroid glands.
4. In patients with inconclusive imaging the indication for surgery remains.

The most recent recommendation on imaging techniques for preoperative localisation of PTA was published in Journal of the American College of Radiology (ACR) in November 2021 (79). This recommendation is also fairly general, but somewhat more specific regarding the appropriate imaging options in different situations, although they also state "There is no universally accepted algorithm for parathyroid imaging".

2.2 META-ANALYSES

There are 18 meta-analyses reporting on the performance of preoperative localisation for different modalities, summarised in **Table 2.1**.

When evaluating the results of these meta-analyses, it is important to keep in mind and reflect on the great heterogenicity of the individual clinical studies on which they are based. This applies to differences in study population (especially regarding adenoma size and the gradual change in indication for surgery over time), varying imaging protocols applied for the analysed modalities and variations in the technical performance of the equipment, due to the technical advances over time.

Some of the reported differences in imaging performance are however large enough to be particularly emphasised:

- The difference in sensitivity that can be attributed mainly to different used radiopharmaceuticals, ^{99m}Tc-sestamibi (≈80%), ^{11}C-Methionine (≈80%) and ^{18}F-fluorocholine (≈90%).
- US, 4D-CT, non-enhaced ^{99m}Tc-sestamibi SPECT and ^{11}C-Methionine PET have a sensitivity around 75-80%.
- Contrast-enhanced CT in multimodality imaging (hybrid imaging) seems to increase the sensitivity.
- SVS (sensitivity of 74%) stands out, because of its invasive nature and the fact that it is seldomly used, other than in patients with persistent or recurrent disease, where conventional imaging has been inconclusive or disconcordant.

Imaging method	Year	Studies (n)	Patients (n)	Time span	Sens (CI)	Spec	PPV	Ref
Ultrasonography	2012	19	-	1996-2007	0.76 (0.70-0.81)	-	0.93	(80)
Ultrasonography	2017	12	1137	2001-2012	0.80 (0.77-0.83)	0.77	-	(81)
4D-CT	2017	34	2563	2000-2016	0.73 (0.69-0.78)	-	-	(82)
4D-CT	2020	7	624	2015-2019	0.85 (0.69-0.94)	0.93	-	(83)
4D-CT	2021	5	153	2018-2021	0.77 (0.67-0.86)	-	-	(84)
4D-CT	2021	16	1032	2011-2020	0.75 (0.66-0.82)	0.85	-	(85)
^{99m}Tc-sestamibi Planar	2015	9	-	2006-2014	0.63 (0.51-0.74)	-	0.90	(86)
^{99m}Tc-sestamibi SPECT	2012	9	-	2001-2010	0.79 (0.64-0.91)	-	0.91	(80)
^{99m}Tc-sestamibi SPECT	2015	10	-	2003-2014	0.66 (0.57-0.74)	-	0.82	(86)
^{99m}Tc-sestamibi SPECT/CT	2015	24	1276	2004-2014	0.86 (0.81-0.90)	-	-	(87)
^{99m}Tc-sestamibi SPECT/CT	2015	18	1300	2006-2014	0.84 (0.78-0.90)	-	0.95	(86)
^{99m}Tc-sestamibi SPECT/CT	2016	23	1236	2005-2014	0.88 (0.82-0.92)	-	-	(88)
^{99m}Tc-sestamibi SPECT/CT	2020	7	624	2015-2019	0.68 (0.51-0.82)	0.98	-	(83)
^{99m}Tc-sestamibi SPECT/CECT	2020	5	809	2016-2019	0.87 (0.80-0.92)	0.98	-	(83)
^{11}C-methionine PET	2013	9	258	1994-2011	0.81 (0.74-0.86)	-	-	(89)
^{11}C-methionine PET (10 with LDCT)	2016	14	327	1996-2015	0.69 (0.60-0.78)	-	0.98	(90)
^{11}C-methionine PET (6 with LDCT)	2016	9	137	1998-2015	0.86 (0.77-0.92)	0.86	-	(91)
^{11}C-methionine PET	2021	8	249	2004-2017	0.80 (0.73-0.86)	-	0.95	(92)
^{18}F-choline PET/CT	2018	8	272	2014-2018	0.90 (0.86-0.94)	0.94	-	(93)
^{18}F-choline/^{11}C-choline PET/CT	2018	14	517	2014-2018	0.92 (0.88-0.96)	-	0.92	(94)
^{18}F-choline PET/CT	2020	14	-	2014-2019	0.91 (0.88-0.94)	-	-	(95)
^{18}F-choline PET	2021	14	693	2016-2020	0.92 (0.88-0.95)	-	0.94	(92)
^{18}F-choline PET	2021	5	153	2018-2021	0.89 (0.75-0.98)	-	-	(84)
^{18}F-choline PET/4D-CT	2021	5	153	2018-2021	0.93 (0.78-1.0)	-	-	(84)
^{18}F-choline PET/CT & PET/MRI	2021	10	300	2014-2020	0.96 (0.94-0.98)	-	-	(96)
Selective Venous Sampling (SVS)	2018	12	732	1993-2017	0.74 (0.70-0.78)	-	-	(97)

Table 2.1. *Meta-analysis reporting on the preoperative localisation performance of hyperfunctioning parathyroid glands of different imaging methods in patients with primary hyperparathyroidism. Year, year of publication; Sens, sensitivity; Spec, specificity; PPV, positive predictive value; Ref, reference; LDCT, low dose CT.*

2.3 CLINICAL STUDIES

Some individual studies on ^{99m}Tc-sestamibi SPECT/CT that relates closely to our research are given a brief presentation below:

There are a few recent studies performing head-to head comparison between ^{99m}Tc-sestamibi SPECT combined with non-contrast-enhanced CT (SPECT/NECT) and ^{99m}Tc-sestamibi SPECT combined with contrast-enhanced CT (SPECT/CECT) with remarkably contradictory results.

A retrospective study with 138 patients comparing SPECT with Low-Dose CT (LDCT) and SPECT/CECT reported a per-patient sensitivity of 85.3% and 87.5% and PPV of 95.2% and 100% respectively (98). However, the distribution of adenoma weight for which these results apply was not reported. Further, the reported localisation sensitivity of SPECT/CECT for adenoma < 500 mg was merely 66.7%, which is below the current standards with this technique.

Another retrospective study, based on 31 patients with a median adenoma weight of 400 mg, showed an improvement in per-lesion-based accuracy from 67.7% to 93.5% when adding CECT to SPECT/NECT (99). However, this study was based on a small cohort with no MGD patients. Hence, this result has very limited clinical validity.

A recent retrospective study on 400 patients showed no localisation improvements by adding ^{99m}Tc-sestamibi SPECT to 4D-CT, reporting a sensitivity of 79.3% (4D-CT alone) and 80.4% (combined) (100). Notably, in this cohort there was a higher proportion of MGD patients (19.8%) than the expected prevalence (approximately 10%), which could bias these results. Further, in this study the PTA weight distribution was not reported, hampering the clinical interpretation of this result.

Nichols et al. 2016, using ^{99m}Tc-sestamibi SPECT in combination with LDCT, found significantly lower adenoma weight and lower localisation sensitivity in MGD than in SGD. Interestingly, even in a subgroup of patients with weight matched adenomas, the sensitivity remained lower for patients with MGD than those with SGD, 64% and 98%, respectively (67).

Krakauer M et al. 2016, in a prospective head-to-head comparison of planar imaging with dual tracer subtraction (^{99m}Tc-sestamibi / ^{123}I), dual-phase planar ^{99m}Tc-sestamibi, 4DCT and US, surprisingly concluded that planar dual tracer subtraction resulted in the highest diagnostic accuracy (101). However, the study population in this work had a large median adenoma weight of 665 mg. Hence, it is doubtful whether this favourable outcome would apply to smaller PTAs, for which the partial volume effect greatly reduces the imaging yield in planar scintigraphy.

There are also studies in which imaging and biochemical variables have been combined to predict MGD, however, with limited success (68, 102-105).

Several methods are not yet represented in the current meta-analyses presented above. Performance data from some clinical studies on these modalities are presented below:

Although MRI has existed for several decades, the method has not been systematically assessed in terms of performance regarding localisation of PTAs.
One retrospective study on a heterogenous patient cohort (125 patients) with a mixture of recurrent/persistent and first-time pHPT, reported a sensitivity of 79.9% and a PPV of 84.7%. Other than that, there are merely small studies on cohorts of approximately 25-30 patients, demonstrating a sensitivity around 60-65% (106, 107).
Two studies including dynamic 4D-MRI, on 30 and 11 patients, respectively, have shown excellent results with 93.3% and 90% sensitivity, respectively and 100% specificity in both (107, 108).

There are at least 3 small studies (10,15 and 34 patients, respectively) reporting on the performance of ^{18}F-fluorocholine PET/MRI in patients with prior inconclusive US and ^{99m}Tc-sestamibi scintigraphy. They all reports promising results, although there are some methodological issues, with a mixture of patients performing either PET/CT or PET/MRI in one (109) and a mixture of patients with and without surgical confirmations (110). One study on ^{18}F-fluorocholine PET/MRI with rigorous methodology including 10 patients presents a sensitivity of 90% and PPV 100% (111).

Except for studies on diagnostic performance of different modalities, there is also research on methods aiming to optimise the contrast resolution between PTAs, thyroid tissue and lymph nodes. Examples of this are the studies conducted by Raeymaeckers S et al. 2021, based on multiphase contrast-enhanced CT (112) and by Nael K et al. 2015, based on dynamic MRI angiography for characterising inflow, peak and wash-out of the iv contrast agent (113). Additionally, dual energy CT (4D-DECT) have successfully been used to analyse spectral information to separate these tissues (114-116).

2.4 THE DIFFICULTIES IN DEFINING A STANDARD IMAGING PROCEDURE

There are many reasons for the problem of establishing general recommendations regarding the preoperative imaging procedures for localisation of PTAs. Some probable causes have been listed below.

2.4.1 The variation in availability and capacity

Some of the methods have limited availability in the world and access to some of these is restricted even in the western countries. PET/CT is usually limited to university hospitals. Even within these centres, PET/CT capacity can be a problem as the method is a crucial diagnostic tool in oncological patients who require priority. Also, the availability of the tracers (^{11}C-methionine or ^{18}F-fluorocholine) is still limited. Many parts of the world even lack access to SPECT, CT and MRI.

2.4.2 The comparison of performance reported in clinical studies

There are many studies on the performance of different imaging modalities for preoperative localisation of hyperfunctioning parathyroid glands, yet no detailed consensus on which technique should be regarded as the standard imaging procedure. This could be due to the lack of evidence favouring a specific method with a specific examination protocol. Further there are confounding factors that need to be considered when comparing the study results of different modalities / protocols.

1. *Methodological heterogenicity*. In the literature, the focus has been on performance comparison between modalities with less emphasis on the effect of different examination protocols, which may give a skewed view of a method. As an example, ^{99m}Tc-sestamibi scintigraphy can be performed in many different ways resulting in very varying performance results.
2. *Patient selection bias*. Parathyroid imaging procedures are often executed in a step-wise manner, by which failure of one modality leads to subsequent examination with another method. Hence, there is often a preselection depending on whether a specific method is applied for first-, second- or third-line imaging. Inclusion criteria sometimes even reinforce such bias. For exemple, discordant findings between first-line methods, such as US and ^{99m}Tc-sestamibi SPECT, sometimes constitute a criterion for inclusion in studies on second-line methods. This is likely to negatively effect the performance results of second- and third-line modalities, and similarly their generalisability. This bias, like many others, would probably go unreconised in a meta-analysis
3. *Lack of randomised phase III studies* comparing different techniques with an endpoint related to MIP and cure. The first one (to my knowledge), APACH II is now ongoing (117)
4. *Few head-to-head comparisons* between the same modality but with different imaging protocols for optimisation.

5. *Lack of control for PTA-size*, one of the factors with large impact on imaging performance. A large proportion of all studies neglect to even comment on adenoma weight. It is difficult to compare studies with large difference in median adenoma weight. The prevalence of goitre among the study patients would, at least in endemic areas, be a factor to report or control for, in order to facilitate the interpretation of the study results.
6. Results based on *small cohorts*, statistically underpowered.
7. *High rate of dropouts.* It is not unusal in studies that many patients are referred for imaging without definite intention to perform surgery which causes a high percentage of drop-outs. Non-localised patients may to a greater extent become excluded from surgery. This would cause a selection bias towards reporting the results for those with more successful localisation, and thus overestimate the sensitivity.
8. *Differences in throughput between centra* will probably have an impact.
9. *Time-bias.* The biochemical diagnosis of the disease and the indication for surgery is an evolving field.

The increased biochemical screening in medicine has, at least in the Western world, resulted in earlier detection of pHPT and thus patients with less overt symptoms (2, 3, 6). Epidemiological studies have shown that also patients with biochemically mild pHPT have a long-term risk of developing significant negative effects, including potentially lethal conditions such as cardiovascular events (118). Many of the negative consequences of pHPT in general have proven reversable by performing parathyroidectomy (6, 19, 20) although some effects are still a matter of debate (2). These discoveries may probably have widened the indication for surgery and has over time resulted in surgical removal of smaller and smaller adenomas (**Figure 2.1**) (119, 120). This trend has called for improvements in preoperative localisation, which has been facilitated by the technical advances in imaging. These two examples however probably lies in the lower range of the adenoma weight spectra and a recent multicentre study on 5861 patients from a European cohort of patients undergone parathyroidectomy during 2015-2018 reported a median adenoma weight of 940 mg (121).

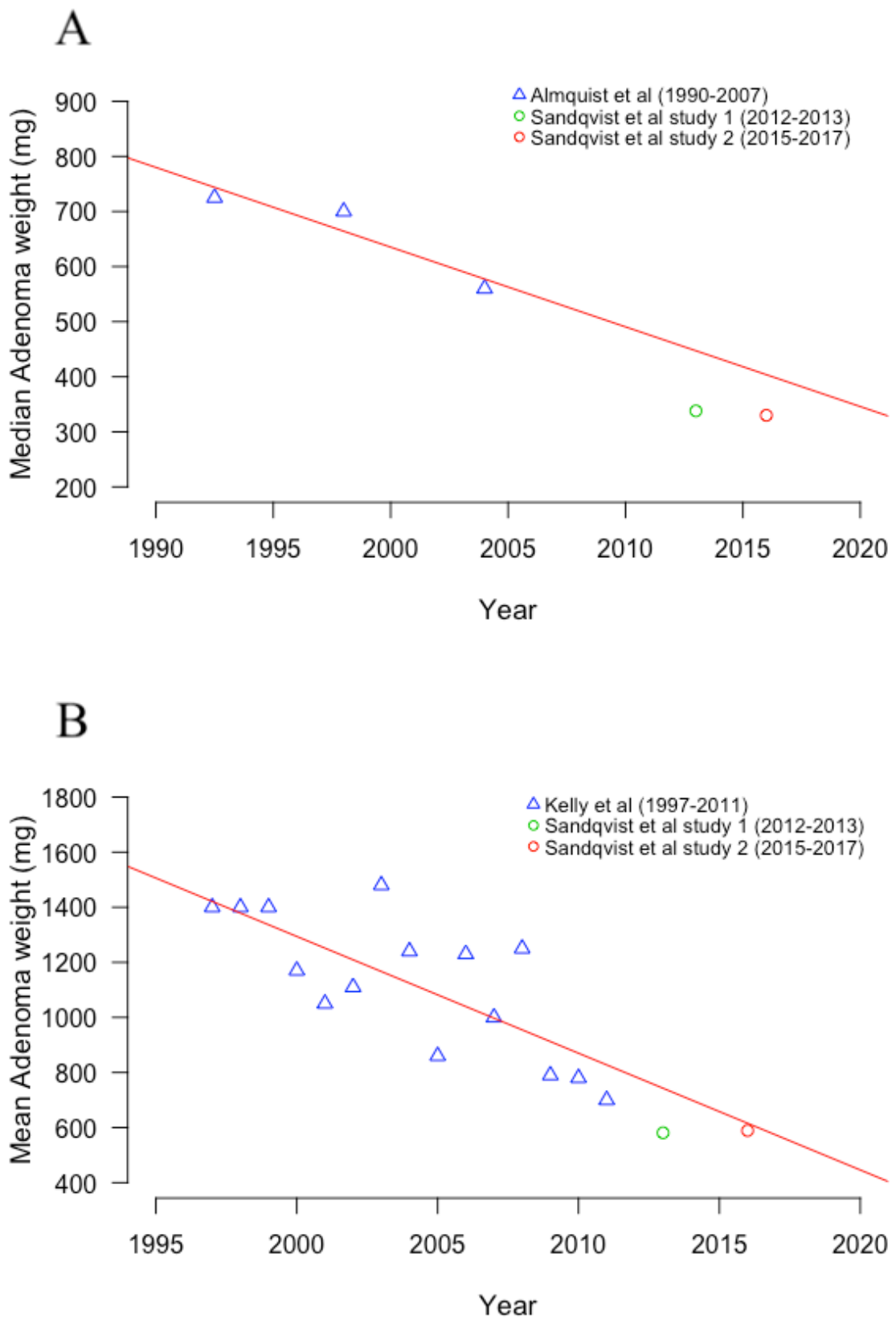

Figure 2.1. *The trend of decreasing adenoma weight over time for surgically removed PTAs in patients with primary hyperparathyroidism from several published cohorts in terms of the median (A) and the mean (B).*

3 RESEARCH AIMS

3.1 THE GENERAL AIM

To improve to diagnostic performance of ^{99m}Tc-sestamibi SPECT/CT for preoperative localisation of hyperfunctioning parathyroid glands and to establish an optimised clinical examination protocol.

3.2 SPECIFIC AIMS

- To assess whether adding a diagnostic nonenhanced CT to ^{99m}Tc-sestamibi SPECT improves PTA localisation performace ***(Study I).***
- To evaluate the gain in diagnostic performance by adding contrast-enhanced CT (arterial and venous phase) to nonenhanced ^{99m}Tc-sestamibi SPECT/CT ***(Study II).***
- To investigate whether ^{99m}Tc-sestamibi SPECT adds to the localisation performance of a multiphase CT ***(Study III).***
- To estimate the influence of the parathyroid adenoma weigth on the localisation performance ***(Study I, II and III).***
- To analyse which CT phases give the largest attenuation difference between parathyroid adenoma and surrounding tissues ***(Study II).***
- To explore whether a machine learning classifier can be trained to predict patients with multiglandular disease in whom only one adeoma was localised at ^{99m}Tc-sestamibi SPECT/CT ***(Study IV).***

4 MATERIALS AND METHODS

4.1 ETHICAL CONSIDERATIONS

With the arrival of a SPECT/CT equipment to our department in June 2012, the clinical routine method for preoperative localisation of PTAs gradually changed from SPECT alone on a conventional gamma camera to nonenhanced SPECT/CT. This decision was made based on earlier studies (122).

All patients included in the studies of this thesis were diagnosed with pHPT based on biochemistry. An endocrine surgeon evaluates the clinical indication for surgery and the need for preoperative localisation before referring the patient to the nuclear medicine department for a routine ^{99m}Tc-sestamibi SPECT/CT.
In ***Study I***, a retrospective quality control was set up to evaluate possible gain in PTA localisation, moving from SPECT alone to the use of combined non-contrast-enhanced SPECT/CT with diagnostic CT quality. Since the patients in this cohort had already been examined for clinical purpose and was retrospectively recruited, no written consent was needed according to the local ethics committee that approved the study.
In ***Study II***, we planned to prospectively evaluate the addition of contrast-enhanced CT (arterial and venous phase) to the clinical routine protocol. The local ethics committee and the radiation protection committee approved the study and all patients provided written informed consent.
Study III was based entirely on the same cohort as ***Study II***.

S***tudy IV*** was based on the cohorts from both ***Study I*** **and** ***II*** but with additional biochemical data extracted from the patients' medical records. An amendment to the original ethical application was approved by the ethics committee.

4.2 PATIENT COHORTS

4.2.1 Study I

The 249 subjects of the first retrospective study were consecutively analysed. Inclusion criteria were biochemical evidence of primary hyperparathyroidism and for clinical purpose having undergone non-contrast-enhanced, dual timepoint ^{99m}Tc-sestamibi SPECT/CT during the period June 2012 to September 2013. We had to exclude 49 patients, mainly because of no surgery performed (38 patients) but also negative surgical outcome with persistent disease, non-coherence between surgery and histopathology or for CT-technical reasons. Altogether 200 patients were analysed.

4.2.2 Study II

The second cohort was prospectively recruited. Exclusion criteria were prior adverse effect from iodine contrast agents, previous neck surgery, renal failure, age < 40 years, referrals

from other sites than the department of endocrine surgery and endocrinology at the Karolinska university hospital. Between May 2015 and May 2017, 192 patients were examined. Out of these, 43 were later excluded due to no surgery performed (32 patients), negative surgery or discordant surgery and histopathology, and 149 patients remained for analysis.

4.2.3 Study III

The patient cohort of this study was the same as in ***Study II*** except for two excluded patients: one due to technical reasons (lack of venous phase) and reader bias for the other patient.

4.2.4 Study IV

This study was based on the cohorts from ***Study I and II*** (349 patients).

4.3 SPECT/CT ACQUISITION PROTOCOL

Throughout this work, all examinations were performed on a dual-head Siemens Symbia T16 SPECT/CT scanner using ultra-high resolution (UHR) collimators (Siemens Healthcare, Erlangen, Germany). SPECT was performed with 128 x 128 image matrix-size, 4.8 mm pixel spacing, 1.0 zoom factor, 64 projections per head (2.8 degrees apart) and 20 seconds per projection. Image reconstruction was performed with OSEM with 4 iterations, 8 subsets and a Gaussian filter with FWHM=12.00 mm. CT for attenuation correction was obtained with 130 kV and 16 mAs and the diagnostic CT with 130 kV and 40 mAs with dose-modulation and 0.75 mm collimation. Scanning length for CT in native phase and contrast-enhanced phases were 40 cm and 25 cm, respectively.

The associated radiation doses for the different studies of this thesis are shown in **Table 4.1**.

	Effective dose (mSv) Study I	Effective dose (mSv) Study II
^{99m}Tc-sestamibi	4,5	4,5
AC-CT	1	1
Native phase	6	6
Arterial phase	n.a.	4
Venous phase	n.a.	4
Total	11,5	19,5

Table 4.1*. The effective radiation dose of each component and in total of the ^{99m}Tc-sestamibi SPECT/CT examination in* ***Study I and II,*** *respectively. n.a. = not applicable.*

The image acquisition protocol used throughout this thesis is based on a single tracer dual time point, 10- and 90-minute SPECT and nonenhanced CT (***Study I and II***) followed by contrast-enhanced CT (***Study II***) as shown in Figure **4.1**.

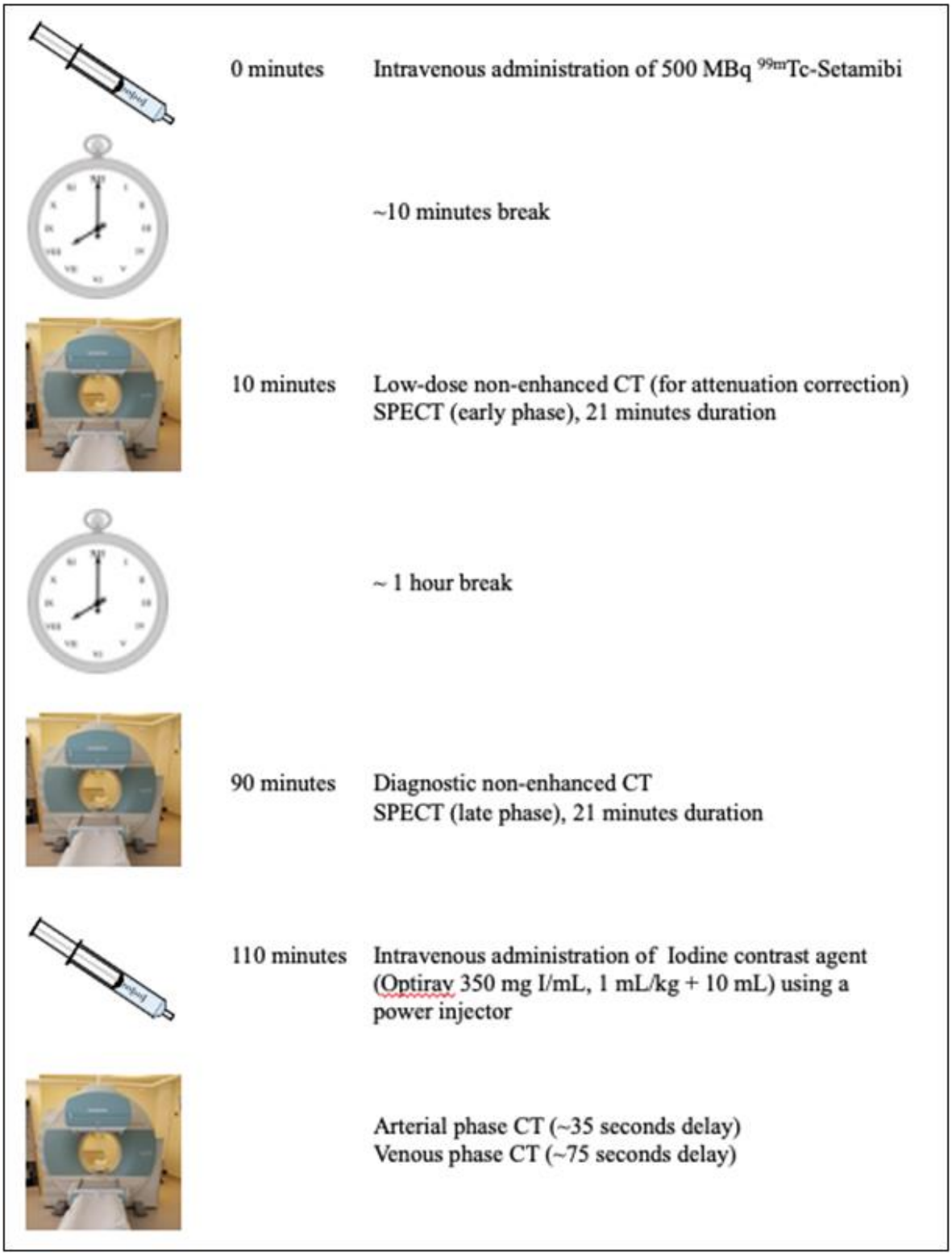

Figure 4.1*. Timeline of SPECT/CT acquisition protocol used in* ***Study II****. The protocol of* ***Study I*** *was identical except it ended after the 90-minute SPECT.*

4.4 IMAGE ANALYSES AND METHODOLOGICAL CONSIDERATIONS

4.4.1 Common approaches for Study I, II and III

In ***Study I, II and III*** of this thesis, we evaluated the role of 4 different components of ^{99m}Tc-sestamibi SPECT/CT for preoperative localisation of PTA. These components were ^{99m}Tc-sestamibi SPECT alone [S], CT with a nonenhanced phase (native) [N], an arterial phase [A] and finally a venous phase [V]. We analysed the performance of 9 defined image sets composed of different combinations of these components [S], [SN], [SNAV], [A], [V], [AN], [VN], [ANS], [VNS]. To assess the added value of a component, the reading of different image sets was for each patient performed sequentially and pairwise, starting with the "simplest" [X] and continuing with more "complex" [XY] to analyse the added value of [Y]. Obviously, all image sets can't without bias be analysed by the reader in one sequence but would require several readers and/or a long "recovery period" to allow for time to make recognition of individual patient cases less likely. Because we lacked experienced readers, we instead chose to divide the analyses into several separate studies, with either a new cohort or a change of readers.

For PTA image localisation, the following main radiomics were considered:

- Typical anatomical position near the posterior aspect of the thyroid gland or adjacent to its upper or lower poles.
- Focal ^{99m}Tc-sestamibi uptake, especially if separated anatomically or by intensity from the thyroid uptake.
- Slower ^{99m}Tc-sestamibi wash-out than that from the thyroid.
- Lower CT attenuation than the thyroid in the native phase.
- Moderate to strong contrast enhancement on CT in arterial phase and a slight washout in the venous phase (123).

In addition to these typical features, parathyroid adenomas may occur in many different forms and can be located at unusual anatomical sites, as described in the literature review above, making the evaluation more complex.

The radiological reports of the retrospective ***Study I*** were not as structured as those for ***Study II***, since these examinations were reported as part of the clinically routine by several radiologists and, at the time, with no intent for scientific assessment.
The radiological reports of the prospective ***Study II***, were considerably more detailed. The location of each finding was described in terms of how the adenoma was related to the anatomical structures, rather than according to the commonly used quadrant terminology (referring to upper and lower pair of parathyroid glands on each side of midline of the neck). In this way a more precise location was described, in relation to for example different parts of the thyroid, trachea, oesophagus, hyoid bone and carotid sheath. Further, the size (mm), ^{99m}Tc-sestamibi uptake (none - high), CT attenuation (low/high in native phase compared to the thyroid) and contrast enhancement (poor – strong) of the findings was also reported.

The evaluation forms (EF) of ***Study I and II*** were quite similar apart from some additional features in Study II, not applicable in Study I concerning tissue-attenuation (HU) in different CT phases.
The main imaging features described in the EF were: Affected parathyroid gland(s) (quadrant/ectopic + additional comments on location similar to radiological report), size in 3 dimensions on CT (mm), ^{99m}Tc-sestamibi uptake (visible yes/no).

In ***Study I-III*** the readers estimated their confidence regarding each finding with a confidence score (CS) from 0-3, also included in the EF. These estimations were not strictly based on imaging criteria, but rather subjectively set but with a unifying theme: 0 – No visible adenoma, 1 – Possibly an adenoma, 2 – Probably an adenoma, 3 – Certainly an adenoma.

Several clinical data were also registered, such us patient characteristics: sex, age, BMI, biochemical profile and surgical parameters: time in the operating room, type of exploration, location of removed PTA (surgical specimen with ID corresponding to PTA in the histopathology report). From the histopathology report also the PTA weights were retrieved.

All image-analyses were performed in a PACS workstation with SECTRA software IDS5-7, Sectra AB, Linköping, Sweden

4.4.2 Study I

A single reader (reader 1), who was blinded for the surgical and pathological reports, firstly evaluated the SPECT alone [S] for all patients. Secondly, the combination of SPECT and diagnostic nonenhanced CT [SN] was assessed.

4.4.3 Study II

In this prospective study, a single reader (reader 1) firstly analysed the nonenhanced SPECT/CT [SN] and registered the findings in the EF. Thereafter, the multiphase SPECT/CT [SNAV] was assessed and registered. The findings of the combined examination (multiphase SPECT/CT) were those reported to the surgeon in the radiological report. The attenuation of the thyroid gland, one lymph node and presumed PTAs, measured in native, arterial and venous phase, respectively, was registered.

4.4.4 Study III

This retrospective study was designed in a more complex way, in order to provide data for multiple objectives. Three readers participated, who all were both radiologist and nuclear medicine physicians. One (reader 1) in the PACS system prepared sets of image presentations for review, and a separate set comprising images with annotations (arrows) revealing the location of the adenoma/adenomas the ground truth (GT) as based on the combined information from [SNAV], surgery and histopathology (further described in 4.4.5 below). The other two readers (reader 2 and 3) were blinded from the results from prior image reading and surgical reports. Both readers reviewed all patients but using different image sets based on either arterial or venous phase for each patient. Thus, reader 2 was provided with

the arterial phase CT [A] for half of the patients and the venous phase CT [V] for the other half of the patients, and vice-versa for reader 3. This "switching" was introduced in order to avoid reader bias. Reading and registration of the findings was performed in a strict consecutive order, starting with either [A] or [V], followed by [AN] or [VN] and finally [ANS] or [VNS].

4.4.5 Linking the anatomical site on radiology to that on surgery for the histopathologically confirmed parathyroid adenoma

To assess the accuracy of the radiological parathyroid adenoma localisation, a chain of reports and events had to be linked. Firstly, long-term normocalcemia (in most cases normal S-Ca^{2+} 6 months postoperatively) was verified to ensure that the patient was cured. Secondly, the histopathologic evaluation of the surgical specimen should confirm a parathyroid adenoma. In that case, its identification number (ID) was then linked to the corresponding ID in the surgical report in order to find the site of removal of that adenoma. Thirdly, the surgical description of that site was compared to the radiologically specified anatomical position in the EF. Finally, an additional correlation check was performed in case of uncertainty, by comparing adenoma weight from the histopathological report and radiological size.

4.4.6 Comparing diagnostic performance in study I, II and III

To test the reasonableness of making a direct comparison of the diagnostic performance of the different methods evaluated in ***Study I, II and III,*** we analysed the demographics of the patients from ***Study I and II*** with regards to patient characteristics including: Age, sex, BMI, biochemical data, operation time, adenoma weight and frequency of MGD. The cohort in ***Study III*** was the same as in ***Study II***, except for two excluded patients, and was therefore assumed equal with regards to patient characteristics.

4.4.7 Study IV

Two response classes were defined in this work:

1. Patients with histopathologically confirmed SGD and with concordant surgical and preoperative imaging localisation (290 patients).
2. Patients with histopathologically confirmed MGD but where only one PTA was correctly localised at preoperative imaging (16 patients).

SGD patients with negative or incorrect ^{99m}Tc-sestamibi SPECT/CT (n=34) as well as MGD patients with complete negative ^{99m}Tc-sestamibi SPECT/CT (n=1) and MGD patients for whom all PTAs were correctly identified on ^{99m}Tc-sestamibi SPECT/CT (n=8) were not included as response classes as extended neck exploration is advisable for these patients in accordance with the clinical practice. Due to the prominent numerical imbalance of these classes risking skewing the training of the MLC, 80 synthetic patients were added to response-class 2 (in total 96), using a previously established synthetic minority over-sampling technique (SMOTE) (124).

As predictors, a set of variables of significance in pHPT were selected:
1. The adenoma weight obtained at histopathological examination of the surgical specimen.
2. A set of biochemical biomarkers: plasma concentration of parathyroid hormone (PTH) and total-calcium (Ca), serum concentration of free ionised calcium (Ca^{2+}) and 24h urine calcium excretion.
3. The plasma concentration of TSH (possibly related to the configuration and activity of the thyroid gland that in turn could affect preoperative imaging using ^{99m}Tc-sestamibi SPECT/CT).

70% of the patients (a mix of real and synthetic) were used for training the MLC and the remaining 30% were used for testing.

In the clinical settings, the true PTA weight is unknown. However, CT image-derived PTA weight has been proven to correlate well with the weight of the surgical specimen (125). Hence, we tested the performance of the trained MLC in a subgroup of patients in the cohort II in whom the weight of the correctly localised PTA could be estimated from volumetric measurements in the contrast-enhanced CT images. For these measurements, the PTA were assumed to have ellipsoid shape and a density of 1 g/ml.

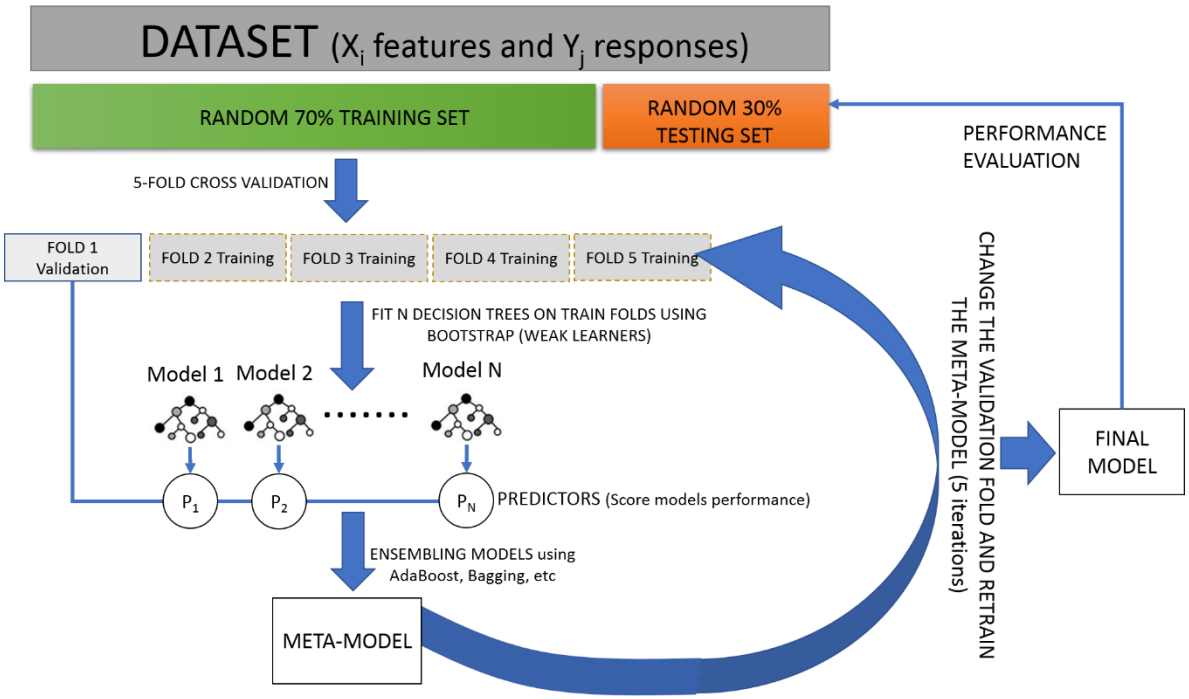

Figure 4.1. *Flowchart of the process of training and testing the machine learning classifier in* ***Study IV****. A 5-fold cross validation was used to iteratively train and validate a classifier based on an ensemble of decision trees.*

4.5 STATISTICAL METHODS

The measurements of the overall diagnostic performance of each image set were calculated on a lesion basis, i.e. as per-adenoma (**Table 4.2**). True negative findings were defined and calculated with the approximation that patients had an average of 4 parathyroid glands and that the glands that were not examined at surgery could be considered normal, since all patients included in the analysis were cured. For MGD, performance per patient was also calculated, for which all adenomas in a patient had to be detected, to be categorised as a true positive patient.

Contingency table			
	PAD +	PAD -	total
SPECT/CT +	TP	FP	TP+FP
SPECT/CT -	FN	TN	TN+FP
total	TP+FN	TN+FP	4*n
Measurements of diagnostic performance			
Sensitivity = TP/(TP+FN)			
Specificity = TN/(TN+FP)			
Accuracy = (TP+TN)/(TP+TN+FP+FN)			
Positive Predictive Value (PPV) = TP/(TP+FP)			
Negative Predictive Value (NPV) = TN/(TN+FN)			
TN - True Negative adenomas = 4*n-(TP+FN+FP)			

***Table 4.2**. Performance measures. TP=True positive adenomas, FN= False Negative adenomas, FP=False Positive adenomas, TN=True Negative adenomas, n = number of patients.*

The confidence interval for each performance measure (binomial proportion confidence interval) was determined using Clopper-Pearson's exact method.
To test for significant difference between paired nominal data for two image sets, McNemar's test was used.
To illustrate the likelihood of correct localisation as a function of the adenoma weight, a binomial logistic regression analysis was performed.
A paired t-test was used to test for differences in attenuation between tissues in several CT phases of the same patient.
To test for differences in demographics between ***Study I and II*** the Mann-Whitney test was used for continuous variables (all non-normally distributed tested using Shapiro-Wilk normality test) and Chi square test of independence for categorial non-pairwise variables.
For the statistical analysis of this thesis, we used: R version 3.6.3 and Matlab version 11.6 release R2021b.

5 RESULTS

5.1 STUDY DEMOGRAPHICS

As shown in **Figure 5.1**, the adenoma weight distribution of cohort I and II was similar and heavily skewed towards low adenoma weight. Patients' characteristics and biochemical abnormalities was essentially the same in ***Study I and II***, except for significantly lower preoperative PTH in ***Study II*** (**Table 5.1**).

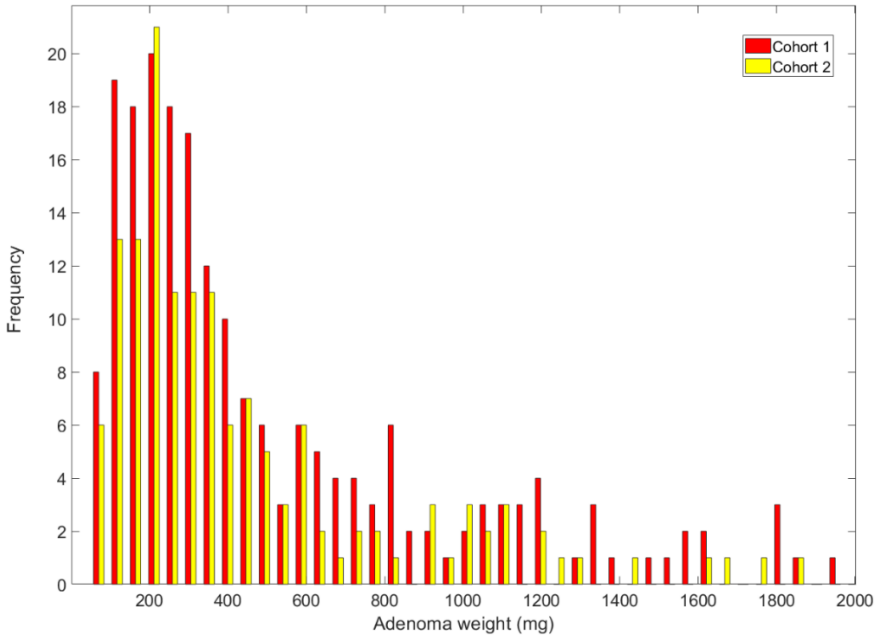

Figure 5.1*. The adenoma weight distribution for the different cohorts of this thesis. Adenomas with weight > 2000 mg are not shown in this figure (7 in* ***Study I*** *and 9 in* ***Study II****).*

	Study I (n=200)	**Study II** (n=149)	p-value
Age (year)	62 (51-71)	63 (54-71)	0.40
Sex (number women)	156/200	111/149	0.45
BMI (kg/m^2**)**	25.3 (22.8-28.7)	25.7 (22.9-28.4)	0.97
PTH (pmol/L)	12 (9.0-15)	9.8 (7.6-13)	<0.001
Ionised Ca^{2+} (mmol/L**)**	1.43 (1.39-1.49)	1.42 (1.39-1.48)	0.40
Creatinine (µmol/L)	69 (60-81)	69 (62-79)	0.61
TSH (mIU/L)	1.60 (1.10-2.20)	1.69 (1.18-2.25)	0.31
Operation time (min)	36 (25-55)	36 (30-52)	0.50
Adenoma weight (mg)	338 (207-745)	330 (200-600)	0.52
Patients with MGD (number)	16/200	9/149	0.48

Table 5.1*. Demographics of the patients retrospectively collected in* ***Study I*** *and those prospectively analysed in* ***Study II****. Values are median (Interquartile range), n= number of patients. An adenoma with the weight 34185 mg has been excluded for data to match that of published data in* ***Study II*** *where mean values were also presented.*

5.2 DIAGNOSTIC PERFORMANCE

The overall head-to-head comparison of the per-lesion based performance between different image sets of this thesis, is shown in **Table 5.2**.

	Study	Sens (%)	p	Spec (%)	p	Acc (%)	p
[S] vs [SN]	I	80.2 vs 82.9	n.s	93.5 vs 95.9	**	89.9 vs 92.4	**
[SN] vs [SNAV]	II	81.1vs 89.9	**	95.9 vs 97.9	n.s	91.9 vs 95.8	***
[A] vs [AN]	III	78.8 vs 80.8	n.s	93.8 vs 96.1	**	89.8 vs 92.0	**
[AN] vs [ANS]	III	80.8 vs 86.5	**	96.1 vs 97.9	n.s	92.0 vs 94.9	***
[A] vs [ANS]	III	78.8 vs 86.5	**	93.8 vs 97.9	***	89.8 vs 94.9	***
[V] vs [VN]	III	73.1 vs 73.7	n.s	92.8 vs 95.6	**	87.6 vs 89.8	*
[VN] vs [VNS]	III	73.7 vs. 80.8	*	95.6 vs 97.7	n.s	89.8 vs 93.2	**
[V] vs [VNS]	III	73.1 vs 80.8	*	92.8 vs 97.7	***	87.6 vs 93.2	***
[A] vs [V]	III	78.8 vs 73.1	n.s	93.8 vs 92.8	n.s	89.8 vs 87.6	n.s
[AN] vs [VN]	III	80.8 vs 73.7	n.s	96.1 vs 95.6	n.s	92.0 vs 89.8	n.s
[ANS] vs [VNS]	III	86.5 vs 80.8	n.s	97.9 vs 97.7	n.s	94.9 vs 93.2	n.s
[ANS] vs [SNAV]§	III / II	86.5 vs 90.4	n.s	97.9 vs 97.9	n.s	94.9 vs 95.9	n.s

Table 5.2*. The per-lesion diagnostic performance (sensitivity, specificity, accuracy) for all image sets evaluated in* ***Study I, II and III*** *with head-to-head comparisons of those evaluated in the same study. Single-gland disease and MGD combined. * (p<0.05); ** (p<0.01); *** (p<0.001); n.s, non-significant. § 2 patients were excluded from this image set to match the number in [ANS] from* ***Study III****, as explained in the materials and methods section.*

As shown in **Figure 5.2**, the per-lesion sensitivity of CT-image sets significantly increased when they were combined with ^{99m}Tc-sestamibi SPECT. Further, this figure shows that the localisation sensitivity is not impacted by adding a native phase.

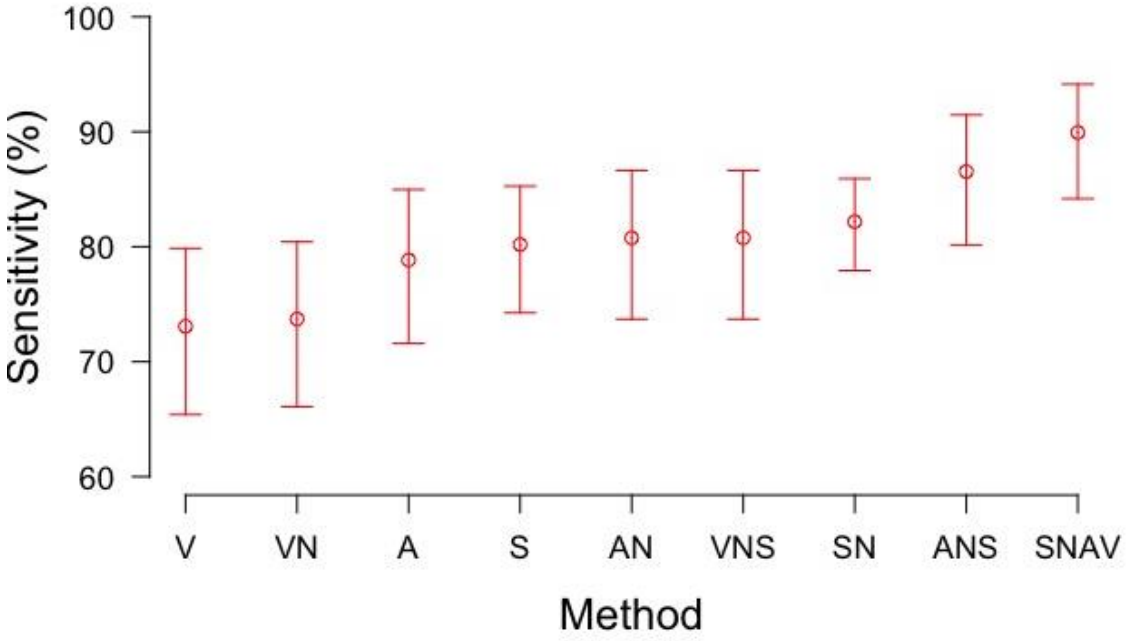

***Figure 5.2**. The sensitivity (95% CI within whiskers) of different image sets evaluated in **Study I**: [S], [SN]; **Study II** [SN], [SNAV] and **Study III** [A], [V], [AN], [VN], [ANS], [VNS]. The result for image set [SN] is the pooled results from **Study I and II**.*

The specificity of the method is important because any false positive findings may lead the surgeon to explore the wrong side of the neck, with subsequent conversion from MIP to BNE, or even worse, removal of this falsely indicated tissue only, resulting in persistent pHPT. As shown in **Figure 5.3**, especially the native phase contributes to increasing the specificity from approximately 93% to 96%.

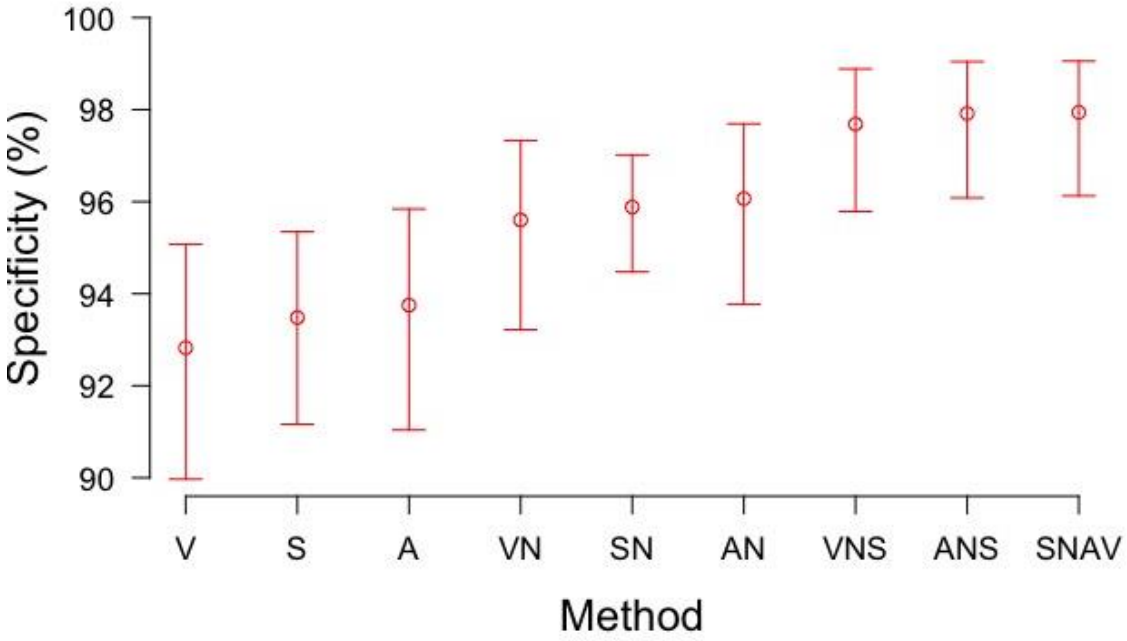

***Figure 5.3**. The specificity (95% CI within whiskers) of different image sets analysed in **Study I**: [S], [SN]; **Study II** [SN], [SNAV] and **Study III** [A], [V], [AN], [VN], [ANS], [VNS]. The result for image set [SN] is the pooled results from **Study I and II**.*

For MGD patients, the per-patient and per-lesion localisation sensitivity for the different image sets used in this thesis, are shown in **Table 5.3**. There was a generally low sensitivity for MGD, for all image sets. However, the specificity was basically 100% for all image sets.

	S	SN I	SN II	SNAV	A	AN	ANS	V	VN	VNS
Patients	16	16	9	9	8	8	8	8	8	8
Patients - all lesions found	0	5	0	3	3	3	3	3	3	3
Per-patient sensitivity (%)	0	31	0	33	38	38	38	38	38	38
Lesions	33	33	19	19	17	17	17	17	17	17
Lesions found	16	20	8	12	10	10	11	11	11	11
Per-lesion sensitivity (%)	49	61	42	63	59	59	65	65	65	65
False positive lesions	0	0	1	0	0	0	0	0	0	0

Table 5.3**. Per-patient and per-lesion based sensitivity for different image sets analysed in **Study I-III in patients with MGD.

5.3 THE IMPACT OF ADENOMA WEIGHT ON THE LIKELIHOOD OF DETECTION

The likelihood of correct localisation is dependent on the weight of the PTA. One way of illustrating this is by applying a binomial logistic regression for the detection rate as a function of the adenoma weight for different examination protocols. As **Figure 5.4** shows, the detection rate is close to 100% for large parathyroid adenomas with a weight of 1000 mg or more, regardless of the localisation method. However, below that the likelihood of detection steeply drops with lower weight. There are however for smaller adenomas large differences in the slope of the curves depending on the examination protocol, with much higher detection rate for contrast-enhanced SPECT/CT than for nonenhanced SPECT/CT or SPECT alone.

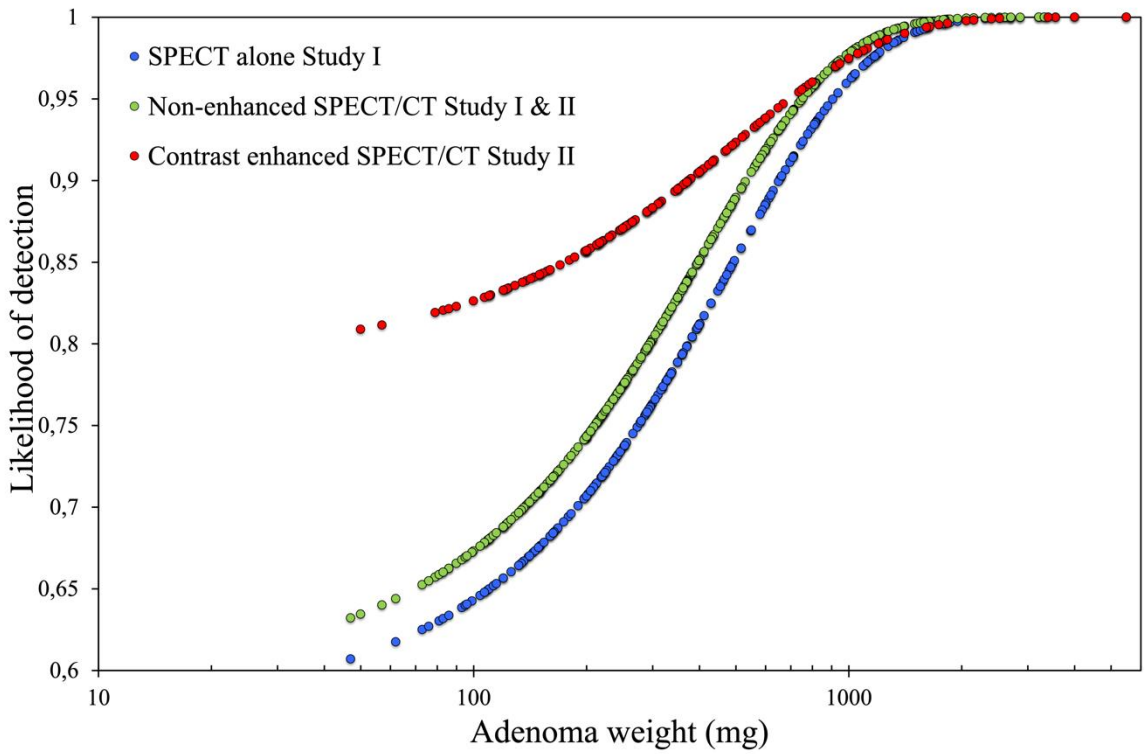

Figure 5.4**. Binomial logistic regression curves illustrating the impact of the adenoma weight on the likelihood of adenoma detection for different SPECT/CT protocols evaluated in **Study I and II.

Figure 5.5 illustrates the large difference in sensitivity of different image sets for small adenomas. The localisation sensitivity for PTA with a weight above the median of the cohorts (338 mg for cohort I and 330 mg for cohort II) is high for all image sets ranging from 86.5-93.3%. However, for small PTAs with weights below the median of the cohorts, the sensitivity is generally much lower 59.5-75.7% except for [ANS] 82.4% and [SNAV] 86.7%. For the two later image sets no statistical difference in sensitivity was found between adenomas with a weight above and below the median ($p = 0.08$ for [ANS] and $p=0.28$ for [SNAV]).

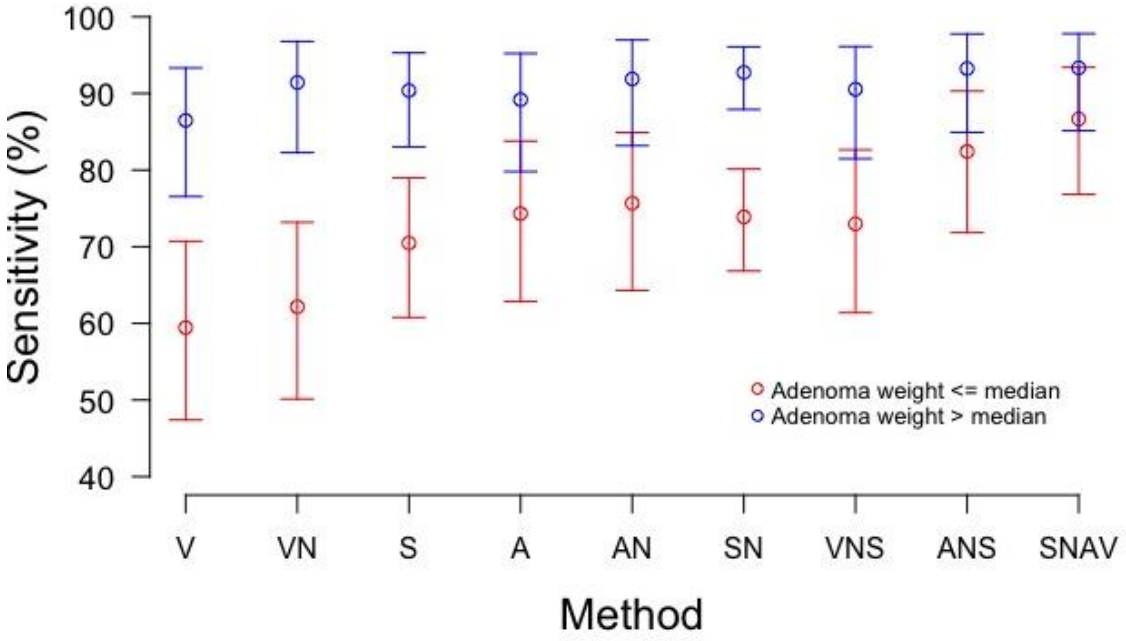

Figure 5.5*. Sensitivity (95% CI within whiskers) of the different image sets for PTAs with weights above and below the median of the cohorts, 338 and 330 mg for cohort I and cohort II, respectively.* ***Study I*** *comprises [S], [SN];* ***Study II*** *[SN], [SNAV] and* ***Study III*** *[A], [V], [AN], [VN], [ANS], [VNS]. The result for image set [SN] is the pooled results from* ***Study I and II****, corresponding to a median adenoma weight of 338 mg.*

5.4 DIFFERENCE IN CT ATTENUATION AND CONTRAST ENHANCEMENT BETWEEN PARATHYROID ADENOMAS, THYROID GLAND AND LYMPH NODES

The distribution of the CT attenuation values (HU) in lymph nodes, PTAs and in the thyroid for different CT phases is illustrated in boxplots in **Figure 5.6**. The difference in attenuation between PTAs, lymph nodes and the thyroid were highly significant in all CT phases ($p<0.001$) except between PTAs and lymph nodes in the native phase. The most pronounced difference in attenuation (HU) between PTAs and the thyroid was found in the native phase, 46 (39,55) and 78 (67,88), median (quartile 1, 3) respectively. The largest difference in attenuation (HU) between PTAs and lymph nodes was found in the arterial phase, 153 (119, 199) and 82 (70, 94), respectively.

The **Figure 5.7** illustrates how these attenuation differences between multiple CT phases are visualised in a representative patient from cohort II. In this example the maximum contrast difference between the thyroid and the PTA was achieved in the native phase, 86 and 56 HU respectively. Likewise, the maximum contrast difference between a lymph node and a PTA was in the arterial phase, 73 and 208 HU, respectively.

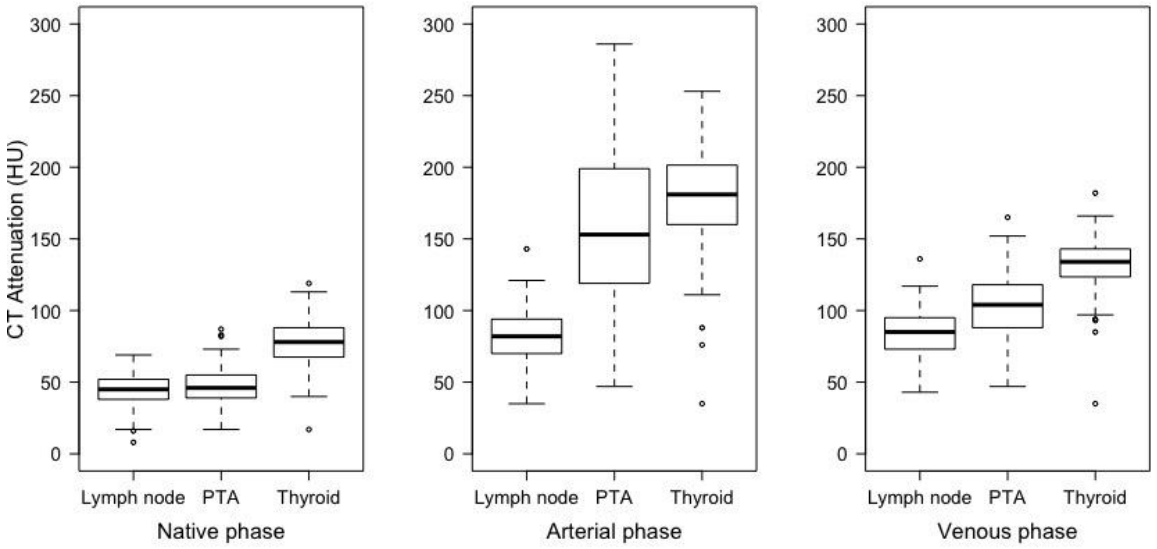

***Figure 5.6**. Boxplots illustrating the variation in CT attenuation of lymph nodes, parathyroid and thyroid tissue in different CT phases analysed in **Study II**.*

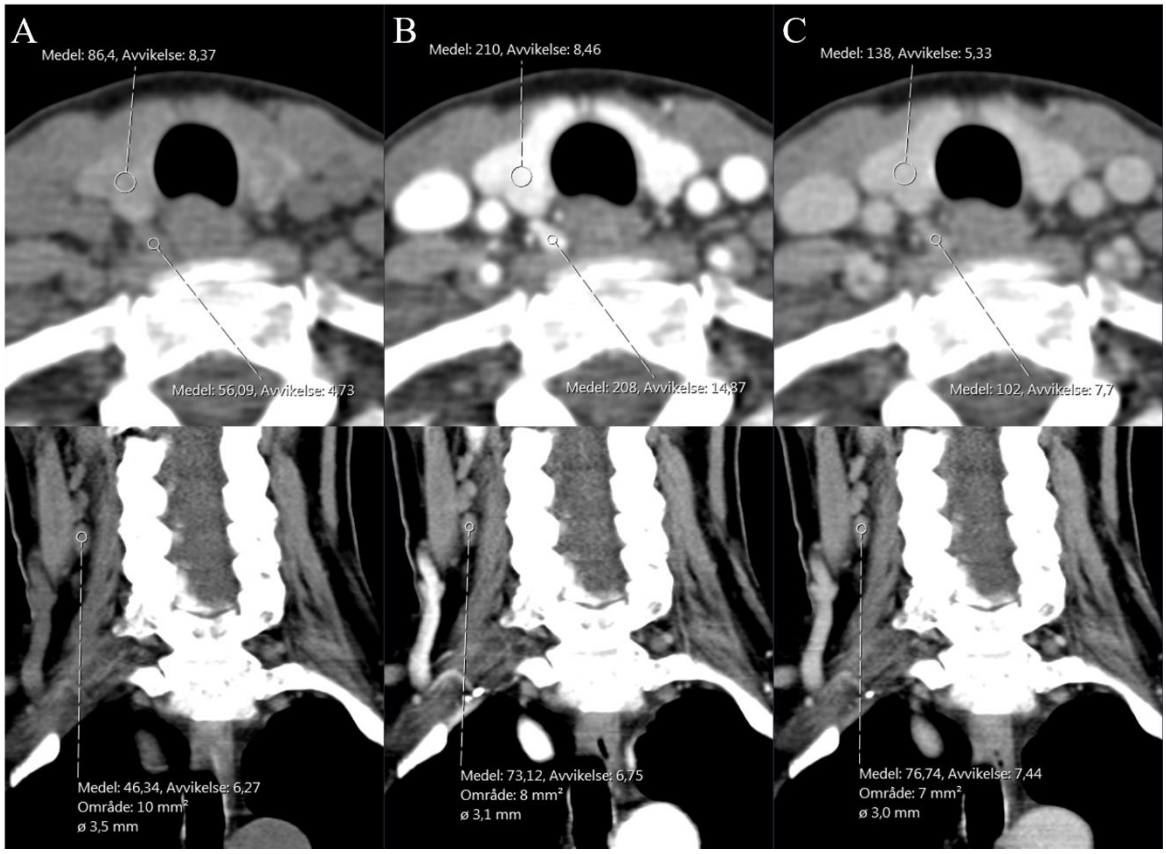

***Figure 5.7**. Transaxial (upper row) and coronal (lower row) CT images in native (A), arterial (B) and venous (C) phases from a representative patient in cohort II. The circles indicate the anatomical structure where the CT attenuation values were measured, the thyroid and parathyroid adenoma in the upper rows and a lymph node in the lower row.*

5.5 THE FREQUENCY AND PPV FOR A GIVEN CONFIDENCE SCORE IN DIFFERENT IMAGE SETS

As shown in **Figure 5.8,** the proportion of true positive findings for a specific CS is constant between different image sets and readers: almost 100% for CS3, 80-85% for CS2 and approximately 55% for CS1 except for [ANS] and [SNAV] in the latter. Furthermore, the proportion of findings scored 3 steeply increases when more imaging modalities are combined, providing complementary information, 32% for [V] and 79% for [SNAV] and without compromising the true positive ratio. For CS1 and CS2 the reversed distribution is seen.

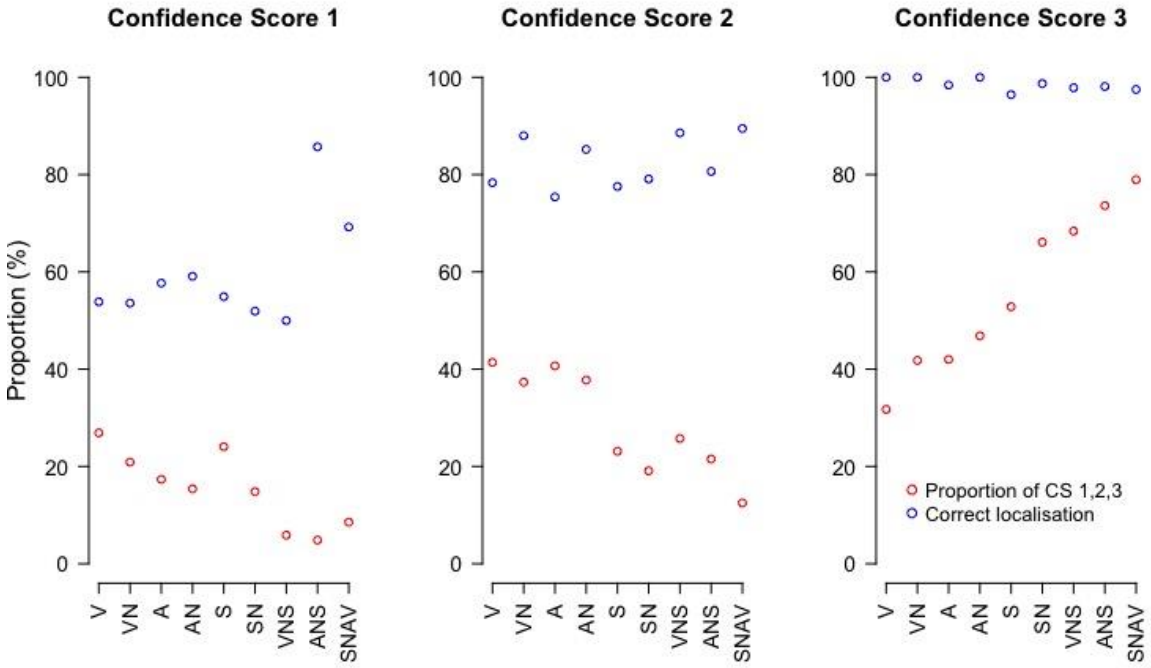

Figure 5.8. The proportion of findings given a certain CS (red circles) and the proportion of true positives (PPV) for these (blue circles), for each image set.

Figure 5.9 shows that the CS for small PTAs (around 300 mg) is low (CS 1 and 2) for all image sets that do not include both a contrast phase and ^{99m}Tc-sestamibi.

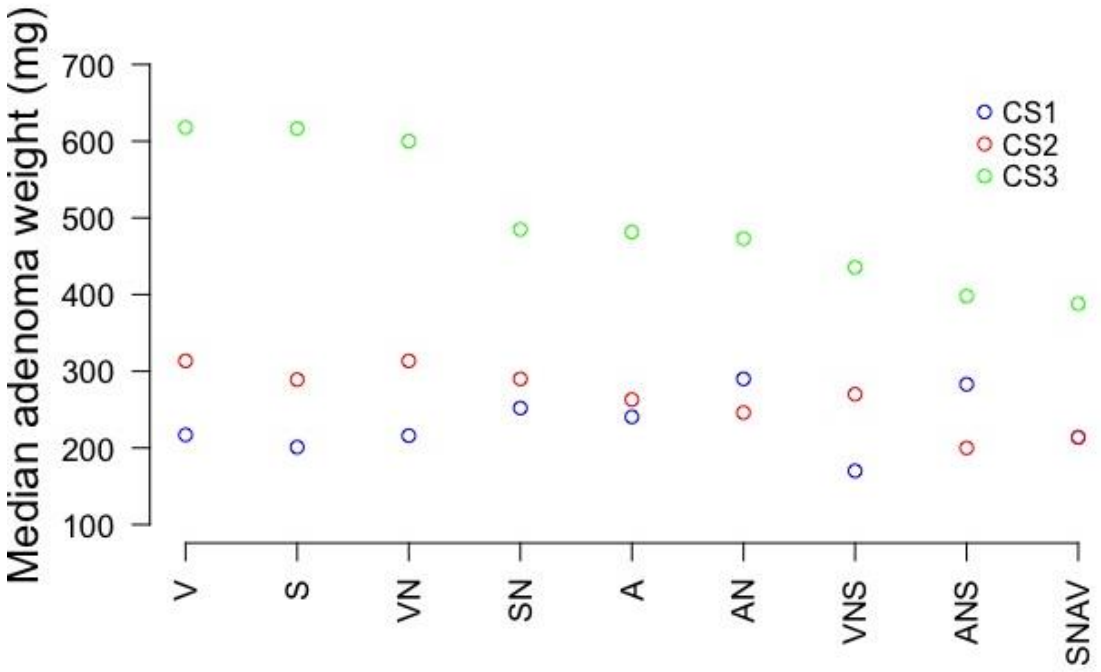

Figure 5.9*. The median adenoma weight by CS and method for correctly detected adenomas.*

5.6 THE PROPORTION OF DIFFERENT SURGICAL EXPLORATION TYPES

Table 5.5 shows the proportion of the different types of surgical explorations. There was a significant difference in the proportion of BNE in ***Study I*** and ***Study II***, 29% and 16% respectively (p=0.042).

Exploration type	Study I		Study II	
	Patients	%	Patients	%
MIP	77	39	78	53
UNE	63	32	45	31
BNE	57	29	24	16

Table 5.5. The number and proportion of patients undergoing different types of surgical exploration in ***Study I*** *and* ***Study II****, respectively.*

5.7 THE PERFORMANCE OF THE MACHINE LEARNING CLASSIFIER

The predictor variables of the two response-classes in ***Study IV*** were similar. Yet, the trained MLC was able to distinguish a significant proportion of patients misclassified as SGD at preoperative imaging without introducing a high rate of false positive MGD, as shown in **Table 5.6**. The performance of the MLC achieved on the training set expressed as the area under the ROC curve (AUC) was 0.9.

	MLC training	MLC testing (1)	MLC testing (2)
Number of patients with SGD	204	86	130
Number of patients with MGD	67	29	6
Fraction	70%	30%	n.a
True Positive Rate (TPR)	80.6%	72.4%	50.0%
False Positive Rate (FPR)	6.9%	5.8%	3.1%

Table 5.6*. The number and fraction of patients used for training and testing the MLC. TPR and FPR for the MLC to predict MGD for patients belonging to any of the defined response classes. Testing (1) – with true adenoma weight; Testing (2) – with image derived adenoma weight.*

6 DISCUSSION

6.1 MAIN RESULTS

In this thesis, we evaluated the different components of ^{99m}Tc-sestamibi SPECT/CT for preoperative localisation in pHPT. In summary we have shown that a native phase [N] contributes to increase the specificity, a contrast-enhanced CT, either arterial phase [A] or venous phase [V] increases the sensitivity but using both seems superfluous and adds to unnecessary radiation exposure to the patient. ^{99m}Tc-sestamibi SPECT [S] contributes with further increased sensitivity.

The adenoma weight has a large impact on the localisation sensitivity, but this effect can be counteracted by combining ^{99m}Tc-sestamibi SPECT and contrast-enhanced CT.

Multiglandular disease remains the main problem in preoperative localisation, regardless of the ^{99m}Tc-sestamibi SPECT/CT-protocol. However, a machine learning classifier (MLC), trained with a few preoperative biochemical parameters, ^{99m}Tc-sestamibi SPECT/CT localisation results and CT image-derived adenoma weight, can assist in identifying MGD-patients misclassified as SGD.

6.2 COMPARISON OF THE IMAGE SETS OF STUDY I - III

To be able to compare the performance of the imaging protocols across ***Study I-III*** we analysed the demographics of the study population in cohort I and II (**Table 5.1**), to ensure that these were similar, and thus not accounting for the demonstrated differences in performance. Patient and adenoma characteristics were essentially the same in study I and II, except for significantly lower preoperative PTH-concentration in the latter. This should however, according to previously published data not significantly affect the sensitivity of ^{99m}Tc-sestamibi SPECT (64, 66).

The examination protocol for [SN] was identical in **Study I** and **II,** and was interpreted by the same reader and, consequently, should result in similar performance in both studies. A test of the reproducibility showed same sensitivity 82.9% vs 81.1% (p=0.75) and similar specificity 95.9% vs 95.9% (p=1) for [SN] in Study I and II. This allowed us to pool the two groups to increase the statistical power.

In ***Study I and II,*** one reader (reader 1) interpreted all examinations allowing for direct (head-to-head) comparison between two image sets. In ***Study III*** two readers (reader 2 and 3) sequentially interpreted 3 image sets, shifting between arterial and venous contrast phase every other patient, which allowed for performance analysis of 6 image sets. Since the cohorts in Study ***II and III*** were identical, we were also able to perform head-to-head comparisons of image sets across studies.

The methodology followed in ***Study III*** did not allow for inter-observer analyses, since the readers reviewed different image sets for the same patient. Instead, one way of assessing differences between readers performance is by doing a head-to-head comparison between

[ANS+VNS for reader 2] vs [VNS + ANS for reader 3]. The overall sensitivity was the same, 85.9% (reader 2) vs 81.4% (reader 3) (p=0.25), but the overall specificity was lower for reader 2, 96.1% (reader 2) vs 99.5% (reader 3) (p=0.0006). This probably reflects the clinical reality and different review approaches for the two readers. Reader 2 seemed to be focused on detecting as many adenomas as possible (high sensitivity) with concomitant lower specificity, while the opposite applies for reader 3.

6.3 THE EFFECT OF THE ADENOMA WEIGHT

Our results clearly show that adenoma weight has a strong impact on localisation performance. **Figure 5.4** illustrates large differences in detection probability for small adenomas between imaging methods, gradually decreasing for larger adenoma weights. The sensitivity curves converge at weight of around 1000 mg, for which all methods perform equally and almost perfect. Furthermore, the effect of adenoma weight on the sensitivity for individual image sets is also large. However, as shown in **Figure 5.5** for image sets containing an arterial phase together with ^{99m}Tc-sestamibi SPECT, localisation performance is independent on PTA weight. Because the biochemical diagnose criteria and the surgical indication may vary among institutions, this result implies that the extent of the preoperative imaging should be adjusted to fit the needs of each clinical site. Altogether, these results also state the importance of presenting of the adenoma weight in all clinical studies concerning preoperative localisation of PTA, since it is crucial for the validity of study results.

6.4 TISSUE CT ATTENUATION AND SESTAMIBI UPTAKE - DIAGNOSTIC PERFORMANCE

As **Figure 5.6** reveals, the largest difference between PTA and thyroid tissue was generally found in the native phase, in which the adenoma attenuation was lower than that in the thyroid. This may explain the significant increase in specificity when adding the native phase [N] to either [A] or [V] (**Figure 5.3**). This helps to avoid interpreting separated bulging or stalked thyroid tissue as a PTA. Further, **Figure 5.6** also shows that the arterial phase provided the largest difference in attenuation between PTA and lymph nodes. This observation might contribute to the increased specificity for [SNAV] compared to [SN] (**Figure 5.3**), although this effect was not statistically significant (borderline). The high contrast enhancement of a PTA (generally well vascularised) in the arterial and venous phases contribute to the increased sensitivity for [SNAV] as compared to [SN] (**Figure 5.2**). Although not specifically studied in this thesis, this sensitivity improvement may be a result of the increasing difference in the contrast-enhanced CT attenuation between the PTA and surrounding fat, muscle, thymic remnants etc. The strong accumulation of ^{99m}Tc-sestamibi in many PTAs, due to the richness of mitochondria in their oxyphilic cell population (**Figure 1.4**), adds significantly to the sensitivity. For patients in whom PTAs do not accumulate enough ^{99m}Tc-sestamibi, have a fast washout or are too small to be detected by the gamma camera, a contrast-enhanced phase is then essential (**Figure 5.2)**. Further, ^{99m}Tc-sestamibi is not only accumulated in PTA but also highly accumulated in many thyroid nodules, brown fat and in lymph nodes affected by granulomatous disease (sarcoidosis etc.), impairing

detection specificity. However, as shown in **Figure 5.3,** adding non-contrast-enhanced CT significantly increases the specificity.

6.5 THE VALUE OF A CONFIDENCE SCORE IN THE IMAGING REPORT

Scoring systems for quantification of various conditions are common in medicine and seems to increase as evaluations become more complex and need to be summitted for the receiver of the assessment.

In ***Study I-III***, the readers scored their confidence of every finding. An objective criteria-based scoring system is probably preferable to our subjective and simple CS. Yet, for the less complex methods it seems to represent the positive predicted value (PPV), regardless of reader, where it could offer a valid quantification and complement the text-based information in the radiological report. However, for the more advanced methods ([ANS] and [SNAV] in **Figure 5.8**), the value of CS seems questionable, since the difference in PPV between CS 1-3 was marginal. Therefore, for these image sets, it might be better to express any uncertainties in a more nuanced way with words.

6.6 RESULT IN THE PERSPECTIVE OF SIMILAR STUDIES

Andersen et al. 2018 (98), with a study-design comparable to ***Study II*** in this thesis, reported similar sensitivities and PPVs for ^{99m}Tc-sestamibi SPECT/CT combined with either nonenhanced low dose CT or with arterial phase contrast-enhanced CT, which contradicts our results. We have shown that there is a statistically significant gain in sensitivity from adding contrast-enhanced CT to ^{99m}Tc-sestamibi SPECT/CT. The fact that Andersen et al. do not report the adenoma weights in their cohort, makes it difficult to compare their results with ours. A plausible explanation could be that their cohort has a larger median adenoma weight for which even SPECT/CT with nonenhanced low-dose CT performs well enough. Noticeable, they report a 67% sensitivity for adenomas smaller than 500 mg in contrast with 82.4% for [ANS] and 86.7% for [SNAV] in our work for adenomas with a weight < 338 mg (**Figure 5.5**).

Yeh et al. 2019 (100) performed a study with a design similar to that of ***Study III*** in this thesis. They performed 4D-CT together with ^{99m}Tc-sestamibi SPECT/CT in a single examination session. They found a 79.3% sensitivity for 4D-CT, 58.0% for ^{99m}Tc-sestamibi SPECT/CT and 80.4% for the two methods combined (Not significant). However, in our ***Study III*** we found 80.8% sensitivity for [AN], which increased to 86.5% by adding ^{99m}Tc-sestamibi SPECT. The different results between these two studies may be explained by the larger proportion of MGD in the study by Yeh et al., almost 20%, as compared to only 6% in our study. MGD is a well-known factor, decreasing the sensitivity of preoperative imaging (64-66), especially of ^{99m}Tc-sestamibi SPECT-alone, which might explain our different conclusion regarding the value of adding ^{99m}Tc-sestamibi SPECT.

6.7 TRADE OFF BETWEEN EXTRA CT PHASES AND RADIATION DOSE

This work aims to optimise the preoperative imaging to maximise PTA localisation performance, with the patient radiation dose as limiting factor (126, 127). In this regard, the diagnostic gain of each imaging component on the overall localisation performance should be weighed against the increased radiation dose. One of the major conclusions of this thesis is that simultaneous use of two contrast-enhanced phases did not improve the performance as compared to only one. An extra CT phase added 4 mSv of radiation dose to the patient (**Table 4.1**). Assuming the linear non-threshold model in which all radiation doses are potentially harmful, this extra dose is then not justifiable (128, 129).

6.8 LIMITATIONS

6.8.1 The impact of imaging on the surgical approach

The results in **Table 5.5**, should be interpreted with caution. Although the decline in BNE between ***Study I and II*** may partly be attributed to the change in preoperative imaging protocol, other clinical factors may also have influenced this result. Examples of factors influencing the choice of surgical approach are, the presence of concomitant goitre, MEN I or II, discordant results at SPECT/CT and US and the criteria for use of ioPTH. Thus, differences between cohort I and II with regards to these factors could influence the results shown in **Table 5.5**. To investigate the net effect of improved preoperative localisation on surgical approach and outcome requires therefore a prospective randomised clinical trial.

6.8.2 Exclusion of patients with preoperative imaging but no surgery

Although imaging is not recommended in patients without the intention of subsequent parathyroidectomy, imaging is sometimes performed anyway. Contraindications to surgery may become apparent at a stage when imaging has already been performed, and sometimes patients change their mind and refuse to undergo surgery, and so on. In our studies ~15% (38/249 patients) in ***Study I*** and ~17% (32/192 patients) in ***Study II*** did not undergo surgery. These "dropout" seems to affect all localisation studies, although they sometimes are completely disregarded.

However, there is a potential risk of introducing a patient selection bias when surgery is cancelled based on a failed preoperative imaging. Thus, resulting in overestimation of the diagnostic performance. Some studies report large exclusion-ratios (mixed causes) of 81% and 46% respectively (130, 131) and others moderate, 28% (100) or low 15% (132) (non-surgical cases). Some studies chose not to report the number of excluded cases (98).
Since our ***Study II*** had a prospective design where an image report of a non-localised case could affect the further indication for surgery, a brief test of this possible effect was performed. There were 8 non-localised patients (25%) in the non-surgery group of 32 patients and 6 (3.8%) in the group of 160 patients who underwent surgery ($p<0.001$), suggesting that the indication for surgery was affected by non-localisation on imaging.

6.8.3 Exclusion of non-cured patients where definitive explanation is lacking

When surgery fails to cure the patient, problems attributable to imaging could be one cause. Incorrect or incomplete localisation (one or more found but in the same patient one or more missed) may mislead the surgeon. The explanation could also be surgical. We could only to a limited extent await reoperations for possible clarification of these failures. A few patients, ~5% (10/211) in ***Study I*** and 7% (11/160) in ***Study II***, for whom clarification was not achieved, were therefor excluded from the imaging performance analyses. This implies that the performance results could be slightly overestimated.

6.8.4 Link between imaging and surgical specimen

Our methodology for linking the anatomical location of the adenoma, established by imaging, with the position at surgical removal and the subsequent histopathological verification, has its weaknesses, but we still favour this more precise anatomical localisation, rather than the commonly used radiological and surgical localisation according to quadrants only. In the latter there is a 25% risk (4 quadrants) for a false positive reported PTA to be counted as a true positive (a false positive link)

6.8.5 Miscellaneous

- A pre-selection is a reality in our institution, with around 27% of the patients solely undergoing US for localisation before surgery. This pre-selection probably concentrate our cohorts to patients with more difficult PTA localisation.
- The exclusion criteria in cohort II might decrease the validity of our findings for certain groups.
- No true interobserver agreement analysis has been performed as our study designs didn't allow that.

6.9 STRENGTHS

- Head-to-head comparison of different protocols. This eliminates many confounding factors.
- Large patient cohorts compared to most individual clinical studies (meta-analysis excluded).
- Evaluation of the impact of adenoma size on preoperative localisation and the reports of the adenoma weight distributions of our cohorts. Few, if any other studies, have more thoroughly presented such data, which are essential for delimiting the population for which the obtained perfomance data is valid.
- Presenting data on dropouts (section 6.8.2).
- The prospective approach of ***Study II***.

6.10 THE MACHINE LEARNING CLASSIFIER

The MLC trained to outline patients with MGD, misclassified as SGD should at this point be recognised only as a proof of concept. It was trained on cohorts with only a limited number of

MGD patients compensated with addition of synthetic patients with similar variance among the predictor variables as in their origin. Thus, the validity of the result may be quite restricted. The MLC should be enriched with additional patients, especially real MGD patients. This may also allow for the recognition of several more response classes that is in this MLC version disregarded or excluded. Furthermore, addition of more image-derived predictors (radiomics) such as the attenuation of the adenoma after administration of contrast media and/or the ^{99m}Tc-sestamibi uptake, may improve the true positive rate of the classifier.

7 CONCLUSIONS

In this thesis we have thoroughly examined the performance of different components of ^{99m}Tc-sestamibi SPECT/CT for preoperative localisation of parathyroid adenoma. We have shown in detail how the performance of the different compositions (examination protocols) of these components (image sets) are dependent on the adenoma weight and that this dependence is pronouncedly reduced for some protocols.

Our results from ***Study I, II and III*** show that an optimal SPECT/CT protocol in a population with median adenoma weight around 330 mg should include: a native phase that contributes to increase specificity, a contrast-enhanced phase (arterial or venous phase) that increases the sensitivity and finally ^{99m}Tc-sestamibi SPECT that further increases the sensitivity.

Despite this optimisation work, complete localisation of all adenomas in patients with MGD remain a significant problem. The **Study *IV*** shows that a machine learning classifier based on a combination of laboratory biomarkers and the CT image-derived PTA weights can accurately predict MGD patients for whom ^{99m}Tc-sestamibi SPECT/CT resulted in localisation of a single adenoma.

8 POINTS OF PERSPECTIVE

- *The potential role of this examination protocol*

^{18}F-fluorocholine has in several studies been shown to be a superior tracer compared to ^{99m}Tc-sestamibi for localisation of PTA and is likely to replace this as the primary method along with ultrasound in some institutions. However, since both ^{99m}Tc-sestamibi and SPECT/CT is more widely available, it will probably remain the mainstay in many secondary centres.

- *The performance of our new clinical SPECT/CT protocol in patients with MGD*

After more than two years using this study protocol, our clinical experience suggest that we are more frequently detecting patients with multiple adenomas. However, it would be of great importance to verify this and the typical image characteristics of these cases in a retrospective study. Such a study would also generate additional data that could improve our machine learning classifier of ***Study IV*** adding new "phenotypes".

- *Randomised clinical trials*

A randomised phase III diagnostic trial (APACH2) is currently conducted in France comparing ^{18}F-fluorocholine PET/CT with ^{99m}Tc-sestamibi SPECT/CT. There is an urge for more studies generating high-level evidence on different imaging methods used for localisation of PTAs.

- *Contrast-enhanced ^{18}F-fluorocholine PET/CT*

The performance of ^{18}F-fluorocholine PET/CT including both a diagnostic nonenhanced CT and contrast-enhanced CT in arterial phase should be further investigated.

- *^{18}F-fluorocholine PET/MRI with dynamic contrast sequence*

To date, there are only a few small studies (10, 26 and 34 patients) that tested ^{18}F-fluorocholine PET/MR (109-111). Only one of them applied a contrast agent (111). Larger studies should be conducted. The method could become an important problem solver in patients with non-localised disease using conventional methods.

9 ACKNOWLEDGEMENTS

Jag har många att framföra min djupaste tacksamhet till, både för direkta bidrag till mitt doktorandprojekt eller indirekt stöd på alla upptänkliga vis. Några omnämns här för ovärderliga insatser, men det finns många fler som på olika sätt bidragit.

Till min huvudhandledare och vän **Alejandro Sanchez-Crespo** för otaliga kreativa diskussioner, gemensamt analyserande och författande, kryddat med lite vänskapligt smågnabb, ett oändligt tack! Du är en fantastisk inspirationskälla när det gäller att presentera resultat på ett såväl vetenskapligt som estetiskt och kondenserat vis, särskilt i visuell form. Jag är skyldig dig rätt många sushi-middagar vid det här laget. Tack också till Jenny, Santi och Rosalia för att ni lånat ut Alex – Det blir sushi till er också!

Anders Sundin – Handledare. Stort tack för all din hjälp att ta mig igenom den snåriga inledande fasen och för all stöttning på vägen när det blåst snålt. Ditt lugn, din vänlighet och ditt tålamod har varit ovärderligt. Inte minst tack för att du under några sommarveckor tog dig tid att granska alla 149 SPECT/CT-undersökningarna i projekt 3.

Inga-Lena Nilsson – Handledare. För alla dina kloka kliniska synpunkter genom kirurgens lupp och för att du hållit oss på rätt kurs när vi i vår iver seglat vilse, mina varmaste tack! Tack också för att vi fått vara medsökande och tilldelats ALF-tid.

Per Grybäck – Handledare och närmaste chef. Tack för ditt stöd och att du trots den inte sällan glesa bemanningen givit mig förutsättningar att ta mig igenom nålsögat. Tack också för ditt vänskapliga kollegiala chefskap och för alla spännande kongresser vi varit på.

Hans Jacobsson – Professor. Tack för att du under så många år tränat mitt nuklearmedicinska öga och för att du dragit in mig i flera projekt som sent omsider ledde fram till mitt eget beslut att påbörja doktorandutbildningen.

Marco Pagani – Min mentor under forskarutbildningen. Tack för förmedling av din livsvisdom, din gästfrihet och för alla kulinariska måltider från det italienska köket som du bjudit mig och Camilla på genom åren.

Jacob Farnebo – Tidigare kollega på nuklearmedicin. Tack för din ihållande uppmuntran beträffande forskningen och för din stora insats att under 2 veckor gå igenom alla patientfallen i projekt 3.

Susanne Fridsten – Kollega och vapendragare på forskarskolan NatiOn III. Tack för din vänskap både under och vid sidan av forskarskolan. Bästa tänkbara organisatör och vän. Tur att jag haft dig att bolla saker med när jag varit förvirrad.

Mina nuvarande läkarkollegor på Nuklearmedicin: Michael Öberg, Erika Bartholdsson, Anna-Klara Sasnauskas, Lisa Kekonius, Carmen Cananau, Sorgul Guven Berk, Helena Sundström, Maja Mladenovic, Anna Kistner, Lennart Blomqvist och tidigare kollegor Cecilia

Wassberg och Saleh Saleh, tack för att ni stöttat och täckt upp för mig under många år så att jag kunnat genomföra mitt avhandlingsarbete och haft överseende när jag varit tyngd av stress.

Jag vill framföra ett stort tack till alla röntgensköterskor på avdelningen och alla i tidbokningen som gjort ett fantastiskt arbete både när det gäller att tillfråga patienter om deltagande i studier, omhändertagande och genomförande av undersökningar.

Jag vill också sända ett varmt tack till kollegorna på den endokrinkirurgiska och endokrinologiska avdelningen för ett gott samarbete.

Ett särskilt tack också till Claes Karlsson, Svetlana Bajalica Lagercrantz och Daria Glaessgen för ert utomordentliga arbete med att organisera den tredje årgången av Nationell forskarskola i klinisk och translationell cancerforskning (NatiOn III 2014-2017).

Till familjen:

Camilla Sandqvist – I nöd och lust heter det i giftas tider. Jag undrar om du hade svarat ja den där augustidagen 2012 om du hade vetat…Hur som helst är jag lycklig över att du fortfarande står vid min sida nu när doktorandutbildningen är i sitt slutskede. Vi har parallellt med detta varit hårt drabbade av mycken sorg, men tillsammans bär vi upp varandra. Vi har också hunnit med att tillsammans renovera tre rum och mycket mer i vårt sommarparadis - timmerhuset som helt saknar räta vinklar. Jag är säker på att både pappa, farmor & farfar, farfars mor och far ler i sin himmel när de ser på vad vi tillsammans åstadkommit. Nu vill jag att vi skall börja skörda av frukterna!

Stig Larsson – Du är oändligt saknad, men ändå alltid med mig. Du har rustat mig inte bara teoretiskt utan minst lika mycket när det gäller det praktiska. Jag är stolt över att slippa ha tummen mitt i handen när jag skall förvalta vår andel av fädernegården.

Anita & Rolf Olofsson – Tack mamma och Rolf för att ni alltid varit trygghetens medelpunkt och för att ni alltid trott på mig, även när jag själv tvivlat! Längtar efter att kunna ses mer nu när Corona verkar gå in i en lugnare fas.

Tack Jennifer Åhman Sandqvist & Thomas Ström och Daniel Sandqvist & Sandra Svensk för att ni finns som bonusbarn i mitt liv. Vad vore meningen med livet om det inte fanns en nästa generation att kämpa för och få hjälp av. Vi har många middagar att ta igen. Daniel du är djupt saknad men alltid med oss!

Tack till våra sju små dvärgar (som inte alla är så små längre) Alexander, Kevin, William, Charlie, Nellie, Lukas och Emilia - för att ni förgyller vår tillvaro. Förlåt att mormor / farmor inte alltid kunnat vara så närvarande som hon önskat, men det skall bli bättre nu.

Birgit, Fredrik, Martin Garmelius & Carolina Björklund – Tack för alla turer till Åfjord laksecamping och alla fina somrar i Jämtland!

Peter, Ulrika, Alexander, Johanna och Adam Larsson - Det är härligt att veta att ni finns, även om det är 50 mil bort och vi alltför sällan ses. Jag hoppas att snart få träffa er uppe i Gäddviken eller nere i Onsala!

10 REFERENCES

1. Seldinger SI. Localization of parathyroid adenomata by arteriography. Acta radiologica. 1954;42(5):353-66.

2. Walker MD, Silverberg SJ. Primary hyperparathyroidism. Nat Rev Endocrinol. 2017.

3. Bilezikian JP, Bandeira L, Khan A, Cusano NE. Hyperparathyroidism. Lancet. 2017.

4. Ruda JM, Hollenbeak CS, Stack BC, Jr. A systematic review of the diagnosis and treatment of primary hyperparathyroidism from 1995 to 2003. Otolaryngol Head Neck Surg. 2005;132(3):359-72.

5. Erickson LA, Mete O, Juhlin CC, Perren A, Gill AJ. Overview of 2022 WHO Classification of Parathyroid Tumors. Endocr Pathol. 2022.

6. Nilsson IL. Primary hyperparathyroidism: should surgery be performed on all patients? Current evidence and residual uncertainties. J Intern Med. 2019;285(2):149-64.

7. Bilezikian JP, Cusano NE, Khan AA, Liu JM, Marcocci C, Bandeira F. Primary hyperparathyroidism. Nat Rev Dis Primers. 2016;2:16033.

8. Vaidya A, Curhan GC, Paik JM, Wang M, Taylor EN. Physical Activity and the Risk of Primary Hyperparathyroidism. The Journal of clinical endocrinology and metabolism. 2016;101(4):1590-7.

9. Marcocci C, Saponaro F. Epidemiology, pathogenesis of primary hyperparathyroidism: Current data. Ann Endocrinol (Paris). 2015;76(2):113-5.

10. Minisola S, Pepe J, Scillitani A, Cipriani C. Explaining geographical variation in the presentation of primary hyperparathyroidism. Lancet Diabetes Endocrinol. 2016;4(8):641-3.

11. Yeh MW, Ituarte PH, Zhou HC, Nishimoto S, Liu IL, Harari A, et al. Incidence and prevalence of primary hyperparathyroidism in a racially mixed population. The Journal of clinical endocrinology and metabolism. 2013;98(3):1122-9.

12. Abood A, Vestergaard P. Increasing incidence of primary hyperparathyroidism in Denmark. Dan Med J. 2013;60(2):A4567.

13. Lappas D, Noussios G, Anagnostis P, Adamidou F, Chatzigeorgiou A, Skandalakis P. Location, number and morphology of parathyroid glands: results from a large anatomical series. Anat Sci Int. 2012;87(3):160-4.

14. Akerstrom G, Malmaeus J, Bergstrom R. Surgical anatomy of human parathyroid glands. Surgery. 1984;95(1):14-21.

15. Agarwal A, Mishra AK, Lombardi CP, Raffaelli M. Applied Embryology of the Thyroid and Parathyroid Glands. Surgery of the Thyroid and Parathyroid Glands2013. p. 15-24.

16. Åkerström G, Stålberg P. Surgical Management of Multiglandular Parathyroid Disease. Surgery of the Thyroid and Parathyroid Glands2013. p. 620-32.

17. Udelsman R, Akerstrom G, Biagini C, Duh QY, Miccoli P, Niederle B, et al. The surgical management of asymptomatic primary hyperparathyroidism: proceedings of the Fourth International Workshop. The Journal of clinical endocrinology and metabolism. 2014;99(10):3595-606.

18. Bilezikian JP, Brandi ML, Eastell R, Silverberg SJ, Udelsman R, Marcocci C, et al. Guidelines for the management of asymptomatic primary hyperparathyroidism: summary statement from the Fourth International Workshop. The Journal of clinical endocrinology and metabolism. 2014;99(10):3561-9.

19. Koman A, Branstrom R, Pernow Y, Branstrom R, Nilsson IL. Prediction of cognitive response to surgery in elderly patients with primary hyperparathyroidism. BJS Open. 2021;5(2).

20. Koman A, Ohlsson S, Branstrom R, Pernow Y, Branstrom R, Nilsson IL. Short-term medical treatment of hypercalcaemia in primary hyperparathyroidism predicts symptomatic response after parathyroidectomy. The British journal of surgery. 2019;106(13):1810-8.

21. Laird AM, Libutti SK. Minimally Invasive Parathyroidectomy Versus Bilateral Neck Exploration for Primary Hyperparathyroidism. Surgical oncology clinics of North America. 2016;25(1):103-18.

22. Kunstman JW, Kirsch JD, Mahajan A, Udelsman R. Clinical review: Parathyroid localization and implications for clinical management. The Journal of clinical endocrinology and metabolism. 2013;98(3):902-12.

23. Hicks G, George R, Sywak M. Short and long-term impact of parathyroid autotransplantation on parathyroid function after total thyroidectomy. Gland Surg. 2017;6(Suppl 1):S75-S85.

24. Versnick M, Popadich A, Sidhu S, Sywak M, Robinson B, Delbridge L. Minimally invasive parathyroidectomy provides a conservative surgical option for multiple endocrine neoplasia type 1-primary hyperparathyroidism. Surgery. 2013;154(1):101-5.

25. Mozzon M, Mortier PE, Jacob PM, Soudan B, Boersma AA, Proye CA. Surgical management of primary hyperparathyroidism: the case for giving up quick intraoperative PTH assay in favor of routine PTH measurement the morning after. Annals of surgery. 2004;240(6):949-53; discussion 53-4.

26. Gunasekaran S, Wallace H, Snowden C, Mikl D, England RJ. Parathyroid ectopia: development of a surgical algorithm based on operative findings. J Laryngol Otol. 2015;129(11):1115-20.

27. Roy M, Mazeh H, Chen H, Sippel RS. Incidence and localization of ectopic parathyroid adenomas in previously unexplored patients. World journal of surgery. 2013;37(1):102-6.

28. Phitayakorn R, McHenry CR. Incidence and location of ectopic abnormal parathyroid glands. American journal of surgery. 2006;191(3):418-23.

29. Koman A, Branstrom R, Pernow Y, Branstrom R, Nilsson IL, Granath F. Neuropsychiatric Comorbidity in Primary Hyperparathyroidism Before and After Parathyroidectomy: A Population Study. World journal of surgery. 2022.

30. Nordenström E. Årsrapport 2018 Scandinavian Quality Register for Thyroid, Parathyroid and Adrenal Surgery (SQRTPA) - http://sqrtpa.se/arsrapporter/. 2018.

31. Socialstyrelsens statistikdatabas för operationer [Available from: https://sdb.socialstyrelsen.se/if_ope/resultat.aspx.

32. Nordenström E. Årsrapport 2020 Scandinavian Quality Register for Thyroid, Parathyroid and Adrenal Surgery (SQRTPA) - http://sqrtpa.se/arsrapporter/. 2020.

33. Singh Ospina NM, Rodriguez-Gutierrez R, Maraka S, Espinosa de Ycaza AE, Jasim S, Castaneda-Guarderas A, et al. Outcomes of Parathyroidectomy in Patients with Primary Hyperparathyroidism: A Systematic Review and Meta-analysis. World journal of surgery. 2016;40(10):2359-77.

34. Jinih M, O'Connell E, O'Leary DP, Liew A, Redmond HP. Focused Versus Bilateral Parathyroid Exploration for Primary Hyperparathyroidism: A Systematic Review and Meta-analysis. Annals of surgical oncology. 2017;24(7):1924-34.

35. Kuzminski SJ, Sosa JA, Hoang JK. Update in Parathyroid Imaging. Magn Reson Imaging Clin N Am. 2018;26(1):151-66.

36. Gasparri G. Updates in primary hyperparathyroidism. Updates Surg. 2017;69(2):217-23.

37. Petranovic Ovcaricek P, Giovanella L, Carrio Gasset I, Hindie E, Huellner MW, Luster M, et al. The EANM practice guidelines for parathyroid imaging. European journal of nuclear medicine and molecular imaging. 2021.

38. Shah R, Gosavi V, Mahajan A, Sonawane S, Hira P, Kurki V, et al. Preoperative prediction of parathyroid carcinoma in an Asian Indian cohort. Head & neck. 2021;43(7):2069-80.

39. Potchen EJ, Wilson RE, Dealy JB, Jr. External parathyroid scanning with Se75 selenomethionine. Annals of surgery. 1965;162(3):492-504.

40. Reitz RE, Pollard JJ, Wang CA, Fleischli DJ, Cope O, Murray TM, et al. Localization of parathyroid adenomas by selective venous catheterization and radioimmunoassay. The New England journal of medicine. 1969;281(7):348-51.

41. Arima M, Yokoi H, Sonoda T. Preoperative identification of tumor of the parathyroid by ultrasonotomography. Surg Gynecol Obstet. 1975;141(2):242-4.

42. Ell PJ, Todd-Pokropek A, Britton KE. Localization of parathyroid adenomas by computer-assisted parathyroid scanning. The British journal of surgery. 1975;62(7):553-5.

43. Doppman JL, Brennan MF, Koehler JO, Marx SJ. Computed tomography for parathyroid localization. Journal of computer assisted tomography. 1977;1(1):30-6.

44. Fukunaga M, Morita R, Yonekura Y, Dokoh S, Yamamoto I, Fujita T, et al. Accumulation of 201Tl-chloride in a parathyroid adenoma. Clinical nuclear medicine. 1979;4(6):229-30.

45. Doppman JL, Krudy AG, Marx SJ, Saxe A, Schneider P, Norton JA, et al. Aspiration of enlarged parathyroid glands for parathyroid hormone assay. Radiology. 1983;148(1):31-5.

46. Stark DD, Moss AA, Gamsu G, Clark OH, Gooding GA, Webb WR. Magnetic resonance imaging of the neck. Part II: Pathologic findings. Radiology. 1984;150(2):455-61.

47. Brasier AR, Wang CA, Nussbaum SR. Recovery of parathyroid hormone secretion after parathyroid adenomectomy. The Journal of clinical endocrinology and metabolism. 1988;66(3):495-500.

48. Nussbaum SR, Thompson AR, Hutcheson KA, Gaz RD, Wang CA. Intraoperative measurement of parathyroid hormone in the surgical management of hyperparathyroidism. Surgery. 1988;104(6):1121-7.

49. Coakley AJ, Kettle AG, Wells CP, O'Doherty MJ, Collins RE. 99Tcm sestamibi--a new agent for parathyroid imaging. Nuclear medicine communications. 1989;10(11):791-4.

50. Taillefer R, Boucher Y, Potvin C, Lambert R. Detection and localization of parathyroid adenomas in patients with hyperparathyroidism using a single radionuclide imaging procedure with technetium-99m-sestamibi (double-phase study). Journal of nuclear medicine : official publication, Society of Nuclear Medicine. 1992;33(10):1801-7.

51. Hellman P, Ahlstrom H, Bergstrom M, Sundin A, Langstrom B, Westerberg G, et al. Positron emission tomography with 11C-methionine in hyperparathyroidism. Surgery. 1994;116(6):974-81.

52. Martinez DA, King DR, Romshe C, Lozano RA, Morris JD, O'Dorisio MS, et al. Intraoperative identification of parathyroid gland pathology: a new approach. Journal of pediatric surgery. 1995;30(9):1306-9.

53. Kaczirek K, Prager G, Kienast O, Dobrozemsky G, Dudczak R, Niederle B, et al. Combined transmission and (99m)Tc-sestamibi emission tomography for localization of mediastinal parathyroid glands. Nuklearmedizin Nuclear medicine. 2003;42(5):220-3.

54. Rodgers SE, Hunter GJ, Hamberg LM, Schellingerhout D, Doherty DB, Ayers GD, et al. Improved preoperative planning for directed parathyroidectomy with 4-dimensional computed tomography. Surgery. 2006;140(6):932-40; discussion 40-1.

55. Mapelli P, Busnardo E, Magnani P, Freschi M, Picchio M, Gianolli L, et al. Incidental finding of parathyroid adenoma with 11C-choline PET/CT. Clinical nuclear medicine. 2012;37(6):593-5.

56. Quak E, Lheureux S, Reznik Y, Bardet S, Aide N. F18-choline, a novel PET tracer for parathyroid adenoma? The Journal of clinical endocrinology and metabolism. 2013;98(8):3111-2.

57. Lezaic L, Rep S, Sever MJ, Kocjan T, Hocevar M, Fettich J. (1)(8)F-Fluorocholine PET/CT for localization of hyperfunctioning parathyroid tissue in primary hyperparathyroidism: a pilot study. European journal of nuclear medicine and molecular imaging. 2014;41(11):2083-9.

58. Chiu ML, Kronauge JF, Piwnica-Worms D. Effect of mitochondrial and plasma membrane potentials on accumulation of hexakis (2-methoxyisobutylisonitrile) technetium(I) in cultured mouse fibroblasts. Journal of nuclear medicine : official publication, Society of Nuclear Medicine. 1990;31(10):1646-53.

59. Zhu M, He Y, Liu T, Tao B, Zhan W, Zhang Y, et al. Factors That Affect the Sensitivity of Imaging Modalities in Primary Hyperparathyroidism. International journal of endocrinology. 2021;2021:1-8.

60. Yang J, Wang H, Zhang J, Xu W, Weng W, Lv S, et al. Sestamibi Single-Positron Emission Computed Tomography/Diagnostic-quality Computed Tomography for the localization of abnormal parathyroid glands in patients with primary

hyperparathyroidism: What clinicopathologic factors affect its accuracy? Journal of endocrinological investigation. 2021;44(8):1649-58.

61. Ishii S, Sugawara S, Yaginuma Y, Kobiyama H, Hiruta M, Watanabe H, et al. Causes of false negatives in technetium-99 m methoxyisobutylisonitrile scintigraphy for hyperparathyroidism: influence of size and cysts in parathyroid lesions. Annals of nuclear medicine. 2020;34(12):892-8.

62. Suter KJL, Johnson W, Yeung M, Serpell J, Lee JC, Grodski S. Surgery for parathyroid microadenomas: patient characteristics, localization success and operative cures. ANZ J Surg. 2018;88(1-2):E21-E4.

63. Galvin L, Oldan JD, Bahl M, Eastwood JD, Sosa JA, Hoang JK. Parathyroid 4D CT and Scintigraphy: What Factors Contribute to Missed Parathyroid Lesions? Otolaryngol Head Neck Surg. 2016;154(5):847-53.

64. Dy BM, Richards ML, Vazquez BJ, Thompson GB, Farley DR, Grant CS. Primary hyperparathyroidism and negative Tc99 sestamibi imaging: to operate or not? Annals of surgical oncology. 2012;19(7):2272-8.

65. Sho S, Yuen AD, Yeh MW, Livhits MJ, Sepahdari AR. Factors Associated With Discordance Between Preoperative Parathyroid 4-Dimensional Computed Tomographic Scans and Intraoperative Findings During Parathyroidectomy. JAMA surgery. 2017.

66. Wachtel H, Bartlett EK, Kelz RR, Cerullo I, Karakousis GC, Fraker DL. Primary hyperparathyroidism with negative imaging: a significant clinical problem. Annals of surgery. 2014;260(3):474-80; discussion 80-2.

67. Nichols KJ, Tronco GG, Palestro CJ. Influence of Multigland Parathyroid Disease on 99mTc-Sestamibi SPECT/CT. Clinical nuclear medicine. 2016;41(4):282-8.

68. Sepahdari AR, Bahl M, Harari A, Kim HJ, Yeh MW, Hoang JK. Predictors of Multigland Disease in Primary Hyperparathyroidism: A Scoring System with 4D-CT Imaging and Biochemical Markers. AJNR American journal of neuroradiology. 2015;36(5):987-92.

69. Shafiei B, Hoseinzadeh S, Fotouhi F, Malek H, Azizi F, Jahed A, et al. Preoperative (9)(9)mTc-sestamibi scintigraphy in patients with primary hyperparathyroidism and concomitant nodular goiter: comparison of SPECT-CT, SPECT, and planar imaging. Nuclear medicine communications. 2012;33(10):1070-6.

70. Pata G, Casella C, Besuzio S, Mittempergher F, Salerni B. Clinical appraisal of 99m technetium-sestamibi SPECT/CT compared to conventional SPECT in patients with primary hyperparathyroidism and concomitant nodular goiter. Thyroid : official journal of the American Thyroid Association. 2010;20(10):1121-7.

71. Joseph K, Berg-Schlosser F, Herbert K. [Computed tomographic determination of thyroid iodine concentration in an endemic goiter area]. Rofo. 1986;144(4):417-21.

72. Bahl M, Sepahdari AR, Sosa JA, Hoang JK. Parathyroid Adenomas and Hyperplasia on Four-dimensional CT Scans: Three Patterns of Enhancement Relative to the Thyroid Gland Justify a Three-Phase Protocol. Radiology. 2015;277(2):454-62.

73. Hunter GJ, Ginat DT, Kelly HR, Halpern EF, Hamberg LM. Discriminating Parathyroid Adenoma from Local Mimics by Using Inherent Tissue Attenuation and Vascular Information Obtained with Four-Dimensional CT: Formulation of a Multinomial Logistic Regression Model. Radiology. 2013.

74. Pandey V, Reis M, Zhou Y. Correlation Between Computed Tomography Density and Functional Status of the Thyroid Gland. Journal of computer assisted tomography. 2016;40(2):316-9.

75. Ye T, Huang X, Xia Y, Ma L, Wang L, Lai X, et al. Usefulness of preoperative ultrasonographic localization for diagnosis of a rare disease: Intrathyroid parathyroid lesions. Medicine (Baltimore). 2018;97(23):e10999.

76. Zafereo M, Yu J, Angelos P, Brumund K, Chuang HH, Goldenberg D, et al. American Head and Neck Society Endocrine Surgery Section update on parathyroid imaging for surgical candidates with primary hyperparathyroidism. Head & neck. 2019;41(7):2398-409.

77. Wilhelm SM, Wang TS, Ruan DT, Lee JA, Asa SL, Duh QY, et al. The American Association of Endocrine Surgeons Guidelines for Definitive Management of Primary Hyperparathyroidism. JAMA surgery. 2016;151(10):959-68.

78. Khan AA, Hanley DA, Rizzoli R, Bollerslev J, Young JE, Rejnmark L, et al. Primary hyperparathyroidism: review and recommendations on evaluation, diagnosis, and management. A Canadian and international consensus. Osteoporos Int. 2017;28(1):1-19.

79. Zander D, Bunch PM, Policeni B, Juliano AF, Carneiro-Pla D, Dubey P, et al. ACR Appropriateness Criteria® Parathyroid Adenoma. Journal of the American College of Radiology. 2021;18(11):S406-S22.

80. Cheung K, Wang TS, Farrokhyar F, Roman SA, Sosa JA. A meta-analysis of preoperative localization techniques for patients with primary hyperparathyroidism. Annals of surgical oncology. 2012;19(2):577-83.

81. Nafisi Moghadam R, Amlelshahbaz AP, Namiranian N, Sobhan-Ardekani M, Emami-Meybodi M, Dehghan A, et al. Comparative Diagnostic Performance of Ultrasonography and 99mTc-Sestamibi Scintigraphy for Parathyroid Adenoma in Primary Hyperparathyroidism; Systematic Review and Meta- Analysis. Asian Pac J Cancer Prev. 2017;18(12):3195-200.

82. Kluijfhout WP, Pasternak JD, Beninato T, Drake FT, Gosnell JE, Shen WT, et al. Diagnostic performance of computed tomography for parathyroid adenoma localization; a systematic review and meta-analysis. European journal of radiology. 2017;88:117-28.

83. Wan QC, Li JF, Tang LL, Lv J, Xie LJ, Li JP, et al. Comparing the diagnostic accuracy of 4D CT and 99mTc-MIBI SPECT/CT for localizing hyperfunctioning parathyroid glands: a systematic review and meta-analysis. Nuclear medicine communications. 2020.

84. Piccardo A, Bottoni G, Boccalatte LA, Camponovo C, Musumeci M, Bacigalupo L, et al. Head-to-head comparison among (18)F-choline PET/CT, 4D contrast-enhanced CT, and (18)F-choline PET/4D contrast-enhanced CT in the detection of hyperfunctioning parathyroid glands: a systematic review and meta-analysis. Endocrine. 2021.

85. Sun L, Yao J, Hao P, Yang Y, Liu Z, Peng R. Diagnostic Role of Four-Dimensional Computed Tomography for Preoperative Parathyroid Localization in Patients with Primary Hyperparathyroidism: A Systematic Review and Meta-Analysis. Diagnostics (Basel). 2021;11(4).

86. Wei WJ, Shen CT, Song HJ, Qiu ZL, Luo QY. Comparison of SPET/CT, SPET and planar imaging using 99mTc-MIBI as independent techniques to support minimally

invasive parathyroidectomy in primary hyperparathyroidism: A meta-analysis. Hell J Nucl Med. 2015;18(2):127-35.

87. Wong KK, Fig LM, Gross MD, Dwamena BA. Parathyroid adenoma localization with 99mTc-sestamibi SPECT/CT: a meta-analysis. Nuclear medicine communications. 2015;36(4):363-75.

88. Treglia G, Sadeghi R, Schalin-Jantti C, Caldarella C, Ceriani L, Giovanella L, et al. Detection rate of (99m) Tc-MIBI single photon emission computed tomography (SPECT)/CT in preoperative planning for patients with primary hyperparathyroidism: A meta-analysis. Head & neck. 2016;38 Suppl 1:E2159-72.

89. Caldarella C, Treglia G, Isgro MA, Giordano A. Diagnostic performance of positron emission tomography using (1)(1)C-methionine in patients with suspected parathyroid adenoma: a meta-analysis. Endocrine. 2013;43(1):78-83.

90. Kluijfhout WP, Pasternak JD, Drake FT, Beninato T, Gosnell JE, Shen WT, et al. Use of PET tracers for parathyroid localization: a systematic review and meta-analysis. Langenbeck's archives of surgery / Deutsche Gesellschaft fur Chirurgie. 2016;401(7):925-35.

91. Yuan L, Liu J, Kan Y, Yang J, Wang X. The diagnostic value of 11C-methionine PET in hyperparathyroidism with negative 99mTc-MIBI SPECT: a meta-analysis. Acta radiologica. 2016.

92. Bioletto F, Barale M, Parasiliti-Caprino M, Prencipe N, Berton AM, Procopio M, et al. Comparison of the diagnostic accuracy of F-18-Fluorocholine PET and C-11-Methionine PET for parathyroid localization in primary hyperparathyroidism: a systematic review and meta-analysis. European journal of endocrinology. 2021;185(1):109-20.

93. Kim SJ, Lee SW, Jeong SY, Pak K, Kim K. Diagnostic Performance of F-18 Fluorocholine PET/CT for Parathyroid Localization in Hyperparathyroidism: a Systematic Review and Meta-Analysis. Horm Cancer. 2018;9(6):440-7.

94. Treglia G, Piccardo A, Imperiale A, Strobel K, Kaufmann PA, Prior JO, et al. Diagnostic performance of choline PET for detection of hyperfunctioning parathyroid glands in hyperparathyroidism: a systematic review and meta-analysis. European journal of nuclear medicine and molecular imaging. 2019;46(3):751-65.

95. Evangelista L, Ravelli I, Magnani F, Iacobone M, Giraudo C, Camozzi V, et al. F-18-choline PET/CT and PET/MRI in primary and recurrent hyperparathyroidism: a systematic review of the literature. Annals of nuclear medicine. 2020;34(9):601-19.

96. Whitman J, Allen IE, Bergsland EK, Suh I, Hope TA. Assessment and Comparison of (18)F-Fluorocholine PET and (99m)Tc-Sestamibi Scans in Identifying Parathyroid Adenomas: A Metaanalysis. Journal of nuclear medicine : official publication, Society of Nuclear Medicine. 2021;62(9):1285-91.

97. Ibraheem K, Toraih EA, Haddad AB, Farag M, Randolph GW, Kandil E. Selective parathyroid venous sampling in primary hyperparathyroidism: A systematic review and meta-analysis. The Laryngoscope. 2018;128(11):2662-7.

98. Andersen TB, Aleksyniene R, Boldsen SK, Gade M, Bertelsen H, Petersen LJ. Contrast-enhanced computed tomography does not improve the diagnostic value of parathyroid dual-phase MIBI SPECT/CT. Nuclear medicine communications. 2018;39(5):435-40.

99. Vu TH, Schellingerhout D, Guha-Thakurta N, Sun J, Wei W, Kappadth SC, et al. Solitary Parathyroid Adenoma Localization in Technetium Tc99m Sestamibi SPECT and

Multiphase Multidetector 4D CT. AJNR American journal of neuroradiology. 2019;40(1):142-9.

100. Yeh R, Tay YD, Tabacco G, Dercle L, Kuo JH, Bandeira L, et al. Diagnostic Performance of 4D CT and Sestamibi SPECT/CT in Localizing Parathyroid Adenomas in Primary Hyperparathyroidism. Radiology. 2019;291(2):469-76.

101. Krakauer M, Wieslander B, Myschetzky PS, Lundstrom A, Bacher T, Sorensen CH, et al. A Prospective Comparative Study of Parathyroid Dual-Phase Scintigraphy, Dual-Isotope Subtraction Scintigraphy, 4D-CT, and Ultrasonography in Primary Hyperparathyroidism. Clinical nuclear medicine. 2016;41(2):93-100.

102. Sho S, Yilma M, Yeh MW, Livhits M, Wu JX, Hoang JK, et al. Prospective Validation of Two 4D-CT-Based Scoring Systems for Prediction of Multigland Disease in Primary Hyperparathyroidism. AJNR American journal of neuroradiology. 2016.

103. Mogollon-Gonzalez M, Notario-Fernandez P, Dominguez-Bastante M, Molina-Raya A, Serradilla-Martin M, Munoz-Perez N, et al. The CaPTHUS score as predictor of multiglandular primary hyperparathyroidism in a European population. Langenbeck's archives of surgery / Deutsche Gesellschaft fur Chirurgie. 2016;401(7):937-42.

104. Mazeh H, Chen H, Leverson G, Sippel RS. Creation of a "Wisconsin index" nomogram to predict the likelihood of additional hyperfunctioning parathyroid glands during parathyroidectomy. Annals of surgery. 2013;257(1):138-41.

105. Kebebew E, Hwang J, Reiff E, Duh QY, Clark OH. Predictors of single-gland vs multigland parathyroid disease in primary hyperparathyroidism: a simple and accurate scoring model. Archives of surgery. 2006;141(8):777-82; discussion 82.

106. Grayev AM, Gentry LR, Hartman MJ, Chen H, Perlman SB, Reeder SB. Presurgical localization of parathyroid adenomas with magnetic resonance imaging at 3.0 T: an adjunct method to supplement traditional imaging. Annals of surgical oncology. 2012;19(3):981-9.

107. Aschenbach R, Tuda S, Lamster E, Meyer A, Roediger H, Stier A, et al. Dynamic magnetic resonance angiography for localization of hyperfunctioning parathyroid glands in the reoperative neck. European journal of radiology. 2012;81(11):3371-7.

108. Merchavy S, Luckman J, Guindy M, Segev Y, Khafif A. 4D MRI for the Localization of Parathyroid Adenoma: A Novel Method in Evolution. Otolaryngol Head Neck Surg. 2016;154(3):446-8.

109. Huber GF, Hullner M, Schmid C, Brunner A, Sah B, Vetter D, et al. Benefit of (18)F-fluorocholine PET imaging in parathyroid surgery. European radiology. 2018;28(6):2700-7.

110. Araz M, Nak D, Soydal C, Peker E, Erden I, Kucuk NO. Detectability of 18F-choline PET/MR in primary hyperparathyroidism. Eur Arch Otorhinolaryngol. 2021.

111. Kluijfhout WP, Pasternak JD, Gosnell JE, Shen WT, Duh QY, Vriens MR, et al. 18F Fluorocholine PET/MR Imaging in Patients with Primary Hyperparathyroidism and Inconclusive Conventional Imaging: A Prospective Pilot Study. Radiology. 2017;284(2):460-7.

112. Raeymaeckers S, De Brucker Y, Vanderhasselt T, Buls N, De Mey J. Detection of parathyroid adenomas with multiphase 4DCT: towards a true four-dimensional technique. BMC medical imaging. 2021;21(1):64-.

113. Nael K, Hur J, Bauer A, Khan R, Sepahdari A, Inampudi R, et al. Dynamic 4D MRI for Characterization of Parathyroid Adenomas: Multiparametric Analysis. AJNR American journal of neuroradiology. 2015;36(11):2147-52.

114. Woisetschlager M, Gimm O, Johansson K, Wallin G, Albert-Garcia I, Spangeus A. Dual energy 4D-CT of parathyroid adenomas not clearly localized by sestamibi scintigraphy and ultrasonography - a retrospective study. European journal of radiology. 2020;124:108821.

115. Bunch PM, Pavlina AA, Lipford ME, Sachs JR. Dual-Energy Parathyroid 4D-CT: Improved Discrimination of Parathyroid Lesions from Thyroid Tissue Using Noncontrast 40-keV Virtual Monoenergetic Images. AJNR American journal of neuroradiology. 2021.

116. Hiebert J, Hague C, Hou S, Wiseman SM. Dual energy computed tomography should be a first line preoperative localization imaging test for primary hyperparathyroidism patients. American journal of surgery. 2018.

117. Quak E, Cardon AL, Ciappuccini R, Lasnon C, Bastit V, Le Henaff V, et al. Upfront F18-choline PET/CT versus Tc99m-sestaMIBI SPECT/CT guided surgery in primary hyperparathyroidism: the randomized phase III diagnostic trial APACH2. BMC endocrine disorders. 2021;21(1):3-.

118. Nilsson IL, Wadsten C, Brandt L, Rastad J, Ekbom A. Mortality in sporadic primary hyperparathyroidism: nationwide cohort study of multiple parathyroid gland disease. Surgery. 2004;136(5):981-7.

119. Almquist M, Bergenfelz A, Martensson H, Thier M, Nordenstrom E. Changing biochemical presentation of primary hyperparathyroidism. Langenbeck's archives of surgery / Deutsche Gesellschaft fur Chirurgie. 2010;395(7):925-8.

120. McCoy KL, Chen NH, Armstrong MJ, Howell GM, Stang MT, Yip L, et al. The small abnormal parathyroid gland is increasingly common and heralds operative complexity. World journal of surgery. 2014;38(6):1274-81.

121. Bergenfelz A, van Slycke S, Makay O, Brunaud L. European multicentre study on outcome of surgery for sporadic primary hyperparathyroidism. The British journal of surgery. 2021;108(6):675-83.

122. Neumann DR, Obuchowski NA, Difilippo FP. Preoperative 123I/99mTc-sestamibi subtraction SPECT and SPECT/CT in primary hyperparathyroidism. Journal of nuclear medicine : official publication, Society of Nuclear Medicine. 2008;49(12):2012-7.

123. Hoang JK, Sung WK, Bahl M, Phillips CD. How to Perform Parathyroid 4D CT: Tips and Traps for Technique and Interpretation. Radiology. 2014;270(1):15-24.

124. Chawala NB, KW; Hall, LO; Kagelmeyer, WP. SMOTE: Synthetic Minority Over-sampling Technique. Journal of Artificial Intelligence Research. 2002;16:321-57.

125. Yeh R, Tay YD, Dercle L, Bandeira L, Parekh MR, Bilezikian JP. A Simple Formula to Estimate Parathyroid Weight on 4D-CT, Predict Pathologic Weight, and Diagnose Parathyroid Adenoma in Patients with Primary Hyperparathyroidism. AJNR American journal of neuroradiology. 2020;41(9):1690-7.

126. Moosvi SR, Smith S, Hathorn J, Groot-Wassink T. Evaluation of the radiation dose exposure and associated cancer risks in patients having preoperative parathyroid localization. Ann R Coll Surg Engl. 2017;99(5):363-8.

127. Hoang JK, Reiman RE, Nguyen GB, Januzis N, Chin BB, Lowry C, et al. Lifetime Attributable Risk of Cancer From Radiation Exposure During Parathyroid Imaging: Comparison of 4D CT and Parathyroid Scintigraphy. AJR American journal of roentgenology. 2015;204(5):W579-85.

128. The 2007 Recommendations of the International Commission on Radiological Protection. ICRP publication 103. Ann ICRP. 2007;37(2-4):1-332.

129. Harding K. ICRP 60 and future legislation. Nuclear medicine communications. 1991;12(9):753-5.

130. Ozkan ZG, Unal SN, Kuyumcu S, Sanli Y, Gecer MF, Ozcinar B, et al. Clinical Utility of Tc-99m MIBI SPECT/CT for Preoperative Localization of Parathyroid Lesions. Indian J Surg. 2017;79(4):312-8.

131. Tunninen V, Varjo P, Kauppinen T, Holm A, Eskola H, Seppanen M. (99m)Tc-Sestamibi/(123)I Subtraction SPECT/CT in Parathyroid Scintigraphy: Is Additional Pinhole Imaging Useful? International journal of molecular imaging. 2017;2017:2712018.

132. Christensen JW, Krakauer M. Added Value of Subtraction SPECT/CT in Dual-Isotope Parathyroid Scintigraphy. Diagnostics (Basel). 2020;10(9):639.